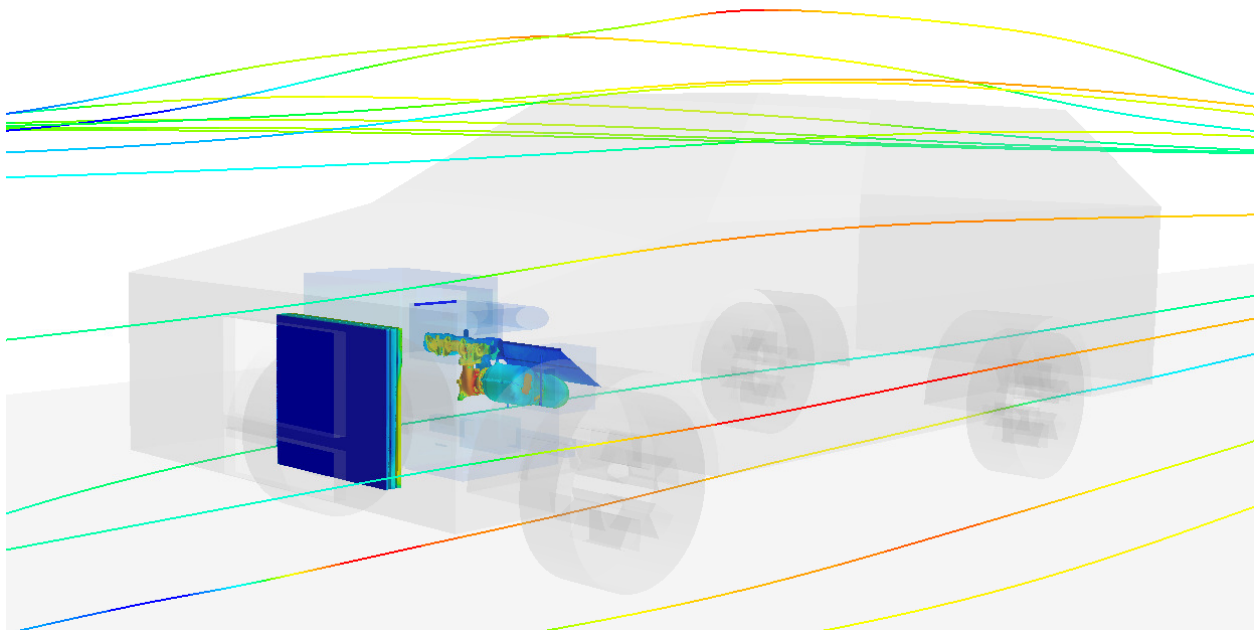




CHALMERS
UNIVERSITY OF TECHNOLOGY



Simulation of transient thermal situation in hill driving using CFD

The development and use of a CFD Semi-Transient method

Master's thesis in Innovative and Sustainable Chemical Engineering

GIULIA MORELLO

MASTER'S THESIS 2018

Simulation of transient thermal situation in hill driving using CFD

The development and use of a CFD Semi-Transient method

GIULIA MORELLO



CHALMERS
UNIVERSITY OF TECHNOLOGY

Department of Chemistry and Chemical Engineering
Division of Chemical Engineering
CHALMERS UNIVERSITY OF TECHNOLOGY
Gothenburg, Sweden 2018

Simulation of transient thermal situation in hill driving using CFD
The development and use of a CFD Semi-Transient method
GIULIA MORELLO

© GIULIA MORELLO, 2018.

Supervisor: Emil Willeson, Volvo Car Corporation, Cooling Performance and Heat Management Department
Examiner: Derek Creaser, Chalmers University of Technology, Chemistry and Chemical Engineering Department

Master's Thesis 2018
Department of Chemistry and Chemical Engineering
Division of Chemical Engineering
Chalmers University of Technology
SE-412 96 Gothenburg
Sweden
Telephone +46 31 772 1000

Cover: Thermal scalar scene of the underhood compartment of a car together with velocity streamlines.

Typeset in L^AT_EX
Chalmers Reproservice
Gothenburg, Sweden 2018

Simulation of transient thermal situation in hill driving using CFD
Master Thesis in Innovative and Sustainable Chemical Engineering
GIULIA MORELLO
Department of Chemistry and Chemical Engineering
Division of Chemical Engineering
Chalmers University of Technology

ABSTRACT

Hill climbing and high load driving condition represents a critical case in which the car may undergo severe stresses. Especially concerning temperatures, the risk of overheating components can be high and the performance of the car can be compromised.

In these cases, CFD tools can be used to simulate the car's behaviour before actually building a prototype, reducing the associated costs. In engineering practice, Steady-State simulations are used, which are based on the assumption of having an infinitely long hill. However, sometimes Steady-State conditions are not reached before the actual hill is finished, with the risk of over-estimating temperatures. Due to the complexity of the model, using transient simulations is almost never an option in daily practice, as they require a high computational demand compared to the time frame of a project work. Therefore, the aim of this project is to develop a Semi-Transient methodology to obtain the same results of a reference transient simulation, but involving a lower computational time demand.

First, the geometry and model were built. Then, Steady State and reference transient simulations were run, followed by four different semi-transient simulations defined by using different time-step and maximum inner iterations values. These four were then compared to the transient case to see which is more accurate. In total four minutes of physical time were simulated.

It was concluded that the semi-transient methodology defined works very well for all the cases, especially for semi-transient 3. Further research should be done on semi-transient simulation 4 and regarding the simulation of minutes beyond minute 5, focusing on the influence of updating the flow field.

Keywords: CFD, underhood, STAR CCM+, ANSA, transient, semi-transient, hill climb, thermal analysis

PREFACE

This report is the result of a 6-months project carried out from January to June 2018 at Cooling Performance and Heat Management Department at Volvo Cars company. The whole project has been performed at the group office in Torslanda. It investigates the definition and implementation of a semi-transient methodology to use as a replacement of the transient one with the aim of consistently reducing the computational time demand. The project was supervised by Emil Willeson at Volvo and examined by Derek Creaser at the Division of Chemical Engineering at Chalmers University of Technology.

ACKNOWLEDGEMENTS

I would like to thank all the people that have contributed to this project through its steps. First, I would like to express my gratitude to my supervisor, Emil Willeson, to have helped me out throughout the all project with his guidance and to have made this experience a great opportunity to learn and enjoy working in Volvo. I would also like to thank my examiner, Derek Creaser, for his support and useful feedback. I want to thank all the people working in Cooling Performance and Heat Management Department to have help me out with their knowledge every time it was needed and to have welcomed me in a friendly and warm environment.

I also would like to thank CD-adapco for giving me the licences to use STAR CCM+ software and in particular I would like to express my gratitude to Jeremy Dahan, for his essential and outstanding support to solve software's issues in an efficient way.

Last but not least, I would like to express my deepest gratitude to my family, friends and to all the people who love me and have always believed in me, from this Earth or from somewhere else. This thesis represents the end of a Master degree that would have been not possible without their persistent support and encouragement.

Sincerely,

Giulia Morello, Gothenburg, June 2018

Nomenclature

Abbreviations

AD	Average Deviation
AE	Absolute Error
AM	Automated Mesh
BC	Boundary Conditions
CAC	Charge Air Cooler
CAE	Computer Aided Engineering
CFD	Computational Fluid Dynamics
FANS	Favre Averaged Navier-Stokes
FF	Freeze Flow
HXC	Heat Exchanger
ME	Maximum Error
MII	Maximum Inner Iterations
MRF	Multiple Reference Frame
MSS	Minimum Surface Sizes
NL	Number of Layers
RANS	Reynolds Averaged Navier-Stokes
RC	Rubber Cylinder
RE	Relative Error
SGR	Surface Growth Rate
SS	Steady State
SW	Surface Wrapping
TS	Time-Step
TSS	Target Surface Sizes
TSTE	Taylor Series Truncation Error
UDS	Upwind Differencing Scheme
VC	Volumetric Control

Greek Symbols

μ	Dynamic viscosity
ν	Kinematic viscosity
ν_T	Eddy turbulent viscosity
ρ	Density
ε	Energy dissipation rate / emissivity
τ_{ij}	Viscous stress tensor
δ_{ij}	Kronecker delta
$\langle \phi \rangle, \bar{\phi}$	Time average of a generic variable
$\tilde{\phi}$	Favre Average of a generic variable

ϕ' Fluctuation of a time-averaged generic variable
 ϕ'' Fluctuation of a Favre-averaged generic variable
 α Absorptivity

Physics Constants

σ Stephan-Boltzmann constant
 g Gravitational Constant
 R Ideal gas Constant

$5.76 \times 10^8 \text{ W} \cdot \text{m}^{-2}$
 $6.67384 \times 10^{-11} \text{ N} \cdot \text{m}^2 \cdot \text{kg}^{-2}$
 $8.3144598, \text{ J} \cdot \text{K}^{-1} \cdot \text{mol}^{-1}$

Other Symbols

A Area of a surface
 C_v Specific heat capacity at constant volume
 e Specific total energy
 k Turbulent kinetic energy / thermal conductivity
 h Convection heat transfer coefficient
 p Pressure
 P_{ij}^V Porous viscous resistance
 P_{ij}^I Porous inertial resistance
 S_{ij} Strain rate tensor
 S_e Energy source term

Contents

Abstract	i
Preface	iii
Acknowledgements	iii
Nomenclature	vi
List of Figures	ix
List of Tables	xi
1 Introduction	1
1.1 Background	1
1.2 Aspects of Relevance	2
1.3 Aim	2
1.4 Limitations	3
1.5 Specification of issue under investigation	4
2 Theory	5
2.1 Fluid Flow Governing Equations	5
2.2 Heat Transfer	6
2.2.1 Conductive heat transfer	6
2.2.2 Convective heat transfer	6
2.2.3 Radiation heat transfer	7
2.3 Turbulence Modeling	7
2.3.1 RANS and FANS	9
2.3.2 Realizable $k - \varepsilon$ Model	9
2.4 Discretization Schemes	10
2.4.1 First order Upwind Scheme	11
2.4.2 Second order Upwind Scheme	11
2.5 Cooling System	11
2.5.1 Condenser	12
2.5.2 Charge Air Cooler	12
2.5.3 Radiator	12
2.5.4 Fan	13
2.6 MRF Fan Modeling	13

2.7	Porous Media Modeling for Heat Exchangers	13
2.8	Geometry Definition and Meshing	14
2.8.1	Clean-Up of the Geometry	14
2.8.2	Volume Meshing	14
2.9	Steady State and Transient Simulations	14
2.9.1	Solution Methodology	15
2.9.2	Residuals	15
3	Methods	19
3.1	Software used	19
3.1.1	ANSA	19
3.1.2	STAR CCM+	19
3.2	Geometry Preparation	20
3.3	Geometry Clean-Up	21
3.4	Volume Meshing	22
3.4.1	Surface Wrapping	23
3.4.2	Surface Remeshing	23
3.4.3	Final Volume Meshing	24
3.5	Model Selection	26
3.6	Boundary Conditions	28
3.6.1	Steady-State Simulations	29
3.6.2	Transient and Semi-Transient Simulations	29
3.7	Solver Settings	30
3.7.1	Steady-State Simulations	31
3.7.2	Reference Transient Simulation	31
3.7.3	Semi-Transient Simulations	33
3.8	Simulations Logic	34
3.8.1	Time Estimations	34
3.8.2	Comparison Method	35
4	Results	39
5	Future Work Suggestions	47
6	Conclusion	49
	Bibliography	51
A	Appendix	I
A.1	Computational Domain	I
A.2	Refinement Blocks	II
A.3	Spheres Position	III

List of Figures

2.1	Velocity decomposition	8
2.2	Main parts in a car's cooling system	12
2.3	Solution methodology in STAR CCM+: outer and inner loops	15
2.4	Typical residuals plot for SS simulations	16
2.5	Typical residuals plot for transient simulations	16
2.6	Example of the importance of setting optimized Time-Step and Maximum Inner Iterations Criteria	17
3.1	Entire simplified car	20
3.2	Simplified underhood compartment	20
3.3	Engine bay and openings	20
3.4	Detailed geometry before geometry clean-up	21
3.5	Detailed geometry after geometry clean-up	21
3.6	Modified engine bay	22
3.7	Final elements inside engine bay	22
3.8	Overall domain, section 1	25
3.9	Car focus, section 1	25
3.10	Overall domain, section 2	25
3.11	Car focus, section 2	26
3.12	Underhood focus, section 1	26
3.13	Underhood focus, section 2	26
3.14	Methodology	28
3.15	Transient and Semi-Transient Step BC	30
4.1	Plot example, sphere 27 01 in heat shield component	39
4.2	Sphere 24 05, exhaust gas component	43
4.3	Sphere 25 02, CAT insulated	43
4.4	Sphere 26 01, CAT non insulated	44
4.5	Sphere 27 08, heat shield component	44
4.6	Zoom of the first 10 seconds, sphere 26 01	45
4.7	Zoom of the first 1.5 seconds, sphere 26 01	46
A.1	Computational Domain, view 1	I
A.2	Computational Domain, view 2	I
A.3	Computational Domain, view 3	II
A.4	Four refinement blocks	II
A.5	Refinement block around the car and its wake	II

A.6 Refinement block around the car's rear and front parts	III
A.7 Air after fan spheres	III
A.8 Exhaust gas spheres	III
A.9 CAT1 insulated spheres	III
A.10 CAT1 non insulated spheres	III
A.11 Spheres for the three RC	IV
A.12 Turbo and manifold spheres	IV
A.13 Heat shield spheres	IV
A.14 Upper absorber spheres	IV
A.15 Lower absorber spheres	IV

List of Tables

3.1	Regions description	23
3.2	Automated Mesh parameters	24
3.3	Blocks and Volumetric Controls	24
3.4	Models for each continua	27
3.5	Materials and emissivities list	27
3.6	SS Boundary Conditions	29
3.7	Transient Boundary Conditions	30
3.8	Final under-relaxation values	31
3.9	Calculation of first tentative Time-Step	32
3.10	Transient Simulation Solver's Settings	33
3.11	Semi-Transient Simulations Solver's Settings	34
3.12	Transient Simulation Times	35
3.13	Semi-Transient Simulations Time	35
3.14	List of scenes printed	36
3.15	List of spheres for further comparison	37
4.1	Air after fan component	40
4.2	Exhaust gas component	40
4.3	CAT insulated area	40
4.4	CAT non insulated area	40
4.5	Turbo and manifold	41
4.6	RC above gear box	41
4.7	RC exhaust-adiabatic box	41
4.8	RC exhaust-turbo	41
4.9	Upper absorbent	41
4.10	Lower absorbent	41
4.11	Heat shield component	41
4.12	Scales used for error classification	42

1

Introduction

1.1 Background

Nowadays, automotive industry is facing many interesting and stimulating challenges. With the aim of producing vehicles with a high standard of performance and design, multiple aspects must be considered. These go from more optional ones, such as high-quality sound system, design and accessories, to more essential ones, such as a high performance of the engine and safety of the vehicle. At Volvo Cars, Cooling Performance and Heat Management Department takes care of the latter aspects and constantly tries to improve them. Over years, standards and features required in cars have been always more strict and demanding. As a result, many components had to be modified or added in the cars' engines, especially in the underhood compartment. To reduce car's noise, modifications were needed such as additional absorber parts and a tighter packaging of mechanical components. For the same purpose, a greater insulation was needed as well [1]. Moreover, with the always more strict CO_2 and other pollutants' emission limits, additional exhaust aftertreatment parts and catalyst had to be added, occupying even more space. Also fuel efficiency has an impact as it creates new heat sources [9]. The use of always more sophisticated electronic devices, the cabin comfort requirements and increased engine power are also other challenging aspects [2]. Considering all these aspects, the underhood area of cars is usually very cramped resulting in complex air flows that pose challenges regarding the thermal aspect of the engine for car designers and engineers [1] [2] [6]. In particular, one of them consists in ensuring that temperatures are within limits. The limits are dictated by different conditions, but mainly they are related to the risk of deterioration or melting of some components in specific hot spots that are formed due to radiation. It is important to limit the overheating of these spots. To avoid these problems, the underhood compartment and the thermal phenomena associated have to be studied and understood [1]. Thermal analysis is of great importance as underhood components are very sensitive to conduction, convection and radiation heat transfer modes. Radiation is very important as temperatures are usually very high, especially near the exhaust manifold and pipes [6].

The thermal analysis is traditionally conducted in wind tunnels tests. However, building car prototypes is highly expensive and many tentatives may be necessary before reaching the desired performance, resulting in a great amount of money to be invested. Moreover, tests are usually time-consuming and if accurate results are desired extreme caution in presetting the instrumentation should be taken as it could interfere with the flow pattern altering it [10]. The idea developed during the last decade is to try to have a design close to its optimum before building the vehicles. This is possible by using numerical tools to execute an appropriate thermal analysis and protection in the early stage of a vehicle development, so

that the optimization of the cooling requirements can be accomplished before building the physical vehicles [7] [14]. Numerical analysis can have many advantages. First, it allows the simulation of different designs and the comparison of them without requiring large materials expenses [9]. Moreover, it allows designers to get a better and more specific understanding of the various components and their inter-connections, helping to identify the parts on which further tests should be focused on [7].

1.2 Aspects of Relevance

Uphill driving conditions with heavy load represent a critical situation from a thermal point of view. Overall, it can be said that even a very slight inclination can affect the temperature distribution in the underhood compartment, as well as influencing the air flow patterns in the car from its openings [2]. In particular, the engine will be subjected to strong efforts and temperatures will be high. According to a study conducted by M. Khaled et al., for uphill driving relative temperature differences due to inclination are more than 4% for many of the underhood components [2]. The risk of temperatures becoming higher than the ones that materials can stand is particularly enhanced in this type of case. It is thus important to check that the integrity of the components is maintained even in extreme conditions [9].

If deterioration or melting of a sensible component takes place, this will affect the quality and the performance of the vehicle in many aspects. Under the costumers aspect, it will expose the drivers to a bad driving experience, but under a more important safety aspect, these problems also pose serious threats to the security of the drivers and of people around as the malfunctioning of the car can cause accidents that can have very serious consequences. Moreover, high temperatures, apart from influencing durability, stresses, deformation and fatigue of components, have an impact on cylinder charge and friction losses and this will influence fuel consumption as well as emissions released to the atmosphere [3] [4]. This is because the cooling system is fundamental to ensure that the engine is operating at its optimal temperature [14]. For all these reasons, many simulations and projects are usually carried out to avoid these problems and keep high standards and performance of cars to offer to the costumers. As transient simulations with the scope of checking the integrity of car components imply a very high computational demand, Volvo Cars decided to start a project to find a faster method to get the same information with a lower computational time demand. They decided to make this project a Master Thesis.

1.3 Aim

In daily practice, simulations are set to steady state (SS) conditions. SS simulations can be used to dimension some car components such as the fan and heat exchanger package and they can give information about long-term temperatures to check the components' integrity. SS simulations are based on the assumption of a infinitely long hill and the reason why these simulations are used is that they involve a relatively low computational time demand. However, in a defined length hill, components may not reach their SS temperatures before the car has ended the hill. Thus SS simulations are associated with the risk of overestimating components' temperatures [5]. Instead, transient simulations are needed to check the

real-time temperatures. The problem associated with this type of simulations is that they involve a high computational demand and time. As an order of magnitude, a transient simulation with a simplified engine may take many weeks to be completed, or even months. The aim of this Thesis is to develop a method that can replace transient simulations for uphill driving conditions with high load, reducing the computational time but maintaining approximately the same accuracy of results obtained. This is achieved by developing a semi-transient method for the simulations, where some simplifications are introduced from the transient case. The heat transfer analysis should comprehend conductive and convective heat transfer modes as well as radiative one [1] [4].

Therefore, the aim of the project is not to represent perfectly the reality, but to develop a Semi-Transient method, allowing some simplifications in the geometry to be introduced. This means that the important thing is that, if simplifications are introduced, they will be the same for the reference transient and semi-transient cases so that they can be compared to see if they produce the same results.

In order to reach the aim, the work has been divided into four parts, following a comparison of the data obtained. Each of the parts will pose the basis for the execution of the next one.

1. Geometry Modelling and Meshing: the geometry to be simulated had to be defined and meshed. The crucial aspect was to decide which level of accuracy the underhood compartment should have. The geometry was modified many times to get an accurate mesh of the areas of interest but maintaining the number of computational cells at a reasonably low value.
2. SS Conditioning: in this phase, SS simulations are run for the conditioning and hill climbing cases. Boundary conditions values were taken from wind tunnel test results.
3. Transient Hill Simulation: this will be the reference transient simulation with which the semi-transient ones will be compared. Transient simulations are not often used in common practice for this case due to the large domain, complex model and very long solving time [6]. The SS conditioning simulation will be the starting file for this simulation.
4. Semi-Transient Hill Simulations: simulations are carried out with the aim to reproduce the same results as the transient one. The concept of semi-transient simulation is based on the use of different solver settings. This will be explained in more details in Chapter 3.

In addition to this, part of the project was also spent to define how the work should proceed in the future stages. This relates which are the aspects to further focus on, which are the targets to accomplish and in which order. The comparison method in this project was also developed so it can be easily updated and used for the future projects.

1.4 Limitations

The main limitation in the project concerns the time limitations imposed by the transient simulation. Due to the high amount of time taken to run the reference transient simulation, it was possible to simulate only one fourth of the physical time decided at first. Moreover, there are two other limitations. First, remembering the aim of the project, some simplifications can

be left in the reference simulation as long as the developed method will have them as well. This is necessary to try to shorten as much as possible the simulation time required. The second limitation comes as an extension of the first one and it concerns the geometry of the engine that will be used in the simulations. As a general statement, it is possible to say that the more precise and detailed the geometry is, the more computational cells will be generated during the meshing phase, and the more time simulations will take to be completed. For this case, a less exact engine geometry could be used without the need of simulating a more detailed and realistic one. However, the geometry cannot be too simplified, as important sensible components whose temperatures are needed to be checked have still to be present. Thus, a trade off has to be made.

1.5 Specification of issue under investigation

Considering the aim of the project, two final research questions can be formulated and their answers will be concluded based on the analysis of results.

Research question 1

Is the semi-transient method effective enough to reproduce transient results?

Research question 2

Which are the next steps to implement for a future continuation of the project?

2

Theory

This chapter is meant to introduce the theoretical knowledge necessary to conduct the thesis and the primary concepts involved in it. First, a description of the fluid flow governing equations is presented along with the different heat transfer modes and their characteristics. Then, turbulence modeling is described in its relevant aspects, followed by a description of the discretization methods. The underhood compartment is then described, with a focus on the cooling system and the possible modelling of its parts. Concepts involved in the definition of the geometry and its meshing are then presented, followed by the definition of SS and transient simulations along with their useful parameters and solver settings.

2.1 Fluid Flow Governing Equations

There are three main equations that characterize the unsteady flow of a fluid: the continuity equation, the momentum equation and the energy equation. Please note that equations below are written for compressible Newtonian fluids. These three equations are mathematical representations of important physical concepts and laws. The continuity equation, shown in (2.1), reflects the law of physics according to which the mass of a fluid is conserved [13].

$$\frac{\partial \rho}{\partial t} + \frac{\partial}{\partial x_i} (\rho u_i) = 0 \quad (2.1)$$

The momentum equation, shown in (2.2), reflects Newton's second law stating that considering a fluid particle, the rate of momentum change is equal to the sum of the forces acting on the particle itself [13].

$$\frac{\partial}{\partial t} (\rho u_i) + \frac{\partial}{\partial x_j} (\rho u_i u_j) = -\frac{\partial p}{\partial x_i} + \frac{\partial \tau_{ij}}{\partial x_j} + \rho f_i \quad (2.2)$$

In (2.2), the term ρf_i represents body force. The term τ_{ij} represents the viscous stresses, which in Newtonian fluids are proportional to the rates of deformation and can be written as:

$$\tau_{ij} = \left(2\mu s_{ij} - \frac{2}{3}\mu \frac{\partial u_k}{\partial x_k} \delta_{ij} \right) \quad (2.3)$$

Where s_{ij} is the strain rate tensor:

$$s_{ij} = \frac{1}{2} \left(\frac{\partial u_i}{\partial x_j} + \frac{\partial u_j}{\partial x_i} \right) \quad (2.4)$$

The energy equation reflects the first law of thermodynamics which states that, considering a fluid particle, the rate of energy change equals the rate of work done and heat added to the fluid particle itself [13]. It can be written as follows, where e is the specific total energy:

$$\frac{\partial}{\partial t}(\rho e) + \frac{\partial}{\partial x_i}(\rho e u_i) = -\frac{\partial}{\partial x_i}(p u_i) + \frac{\partial}{\partial x_i}(\tau_{ij} u_j) + \frac{\partial q_i}{\partial x_i} + \rho u_i f_i + S_e \quad (2.5)$$

In (2.5), S_e represents the energy source term and q_i is the heat flux, which can be described through Fourier's law. The unknown thermodynamic quantities can be derived by using equations of state, that relate other variables to two state variables [13]. For an ideal gas:

$$p = p(\rho, T) = \rho R T \quad (2.6)$$

$$e = e(C_v, T) = C_v T \quad (2.7)$$

where ρ , C_v and R are the gas density, specific heat capacity at constant volume and ideal gas constant respectively.

2.2 Heat Transfer

Heat can be defined as *"the form of energy that can be transferred from one system to another as a result of temperature difference"* [16]. As a matter of fact, it is usually transferred from a high-medium temperature system to a lower temperature one and stops when both the systems reach the same temperature. Heat transfer can occur in three modes: conduction, convection and radiation. Their characteristics and principles are discussed below.

2.2.1 Conductive heat transfer

Conduction is a type of heat transfer that occurs as a result of collisions and consequent diffusion between particles in their random motion. Particles at higher temperatures are associated to a more energetic level and they share and transfer this energy to lower-energy particles, which are at lower temperatures. This generates the heat propagation [16]. Conductive heat transfer can be expressed in its one-dimensional form through Fourier's Law:

$$\dot{Q}_{cond} = -kA \frac{dT}{dx} \quad (2.8)$$

where \dot{Q}_{cond} is the rate of heat conduction through the area A normal to the heat transfer's direction and with thermal conductivity k .

2.2.2 Convective heat transfer

Convection can be defined as the heat transfer that takes place between a solid surface and an adjacent liquid or gas that is in motion. The motion of the fluid enhances the heat transfer, which otherwise will only take place by conduction. Heat convection can be defined either as forced or natural convection. Forced convection takes place when the motion of the fluid is accomplished by external means, such as a pump, the wind or a fan. Natural convection takes place when the motion is generated by the density difference due to the variation of

temperature in the fluid [16]. The convective heat transfer rate is proportional to the difference in temperatures and it is appropriately expressed by Newton's law of cooling:

$$\dot{Q}_{conv} = hA_s(T_s - T_\infty) \quad (2.9)$$

where T_s and T_∞ are the surface and the fluid temperatures respectively, h is the convective heat transfer coefficient and A_s the surface through which the convective heat transfer occurs.

2.2.3 Radiation heat transfer

Radiation is the heat transfer mode that takes place due to energy emissions from bodies via electromagnetic waves. The main difference with the other heat transfer modes is that radiation does not require the presence of any material medium or physical connection and it takes place at a faster rate, which is the speed of light. In this case, the form of radiation that is of interest is the thermal one, in which bodies emit radiation because of their temperatures which is higher than absolute zero. Considering an idealized blackbody, it is possible to express the maximum radiation rate that a body with surface temperature T_s can emit, according to the Stefan-Boltzmann law:

$$\dot{Q}_{emit,max} = \sigma A_s T_s^4 \quad (2.10)$$

where σ is the Stefan-Boltzmann constant. Equation (2.10) is also called the blackbody radiation equation. In reality, the emissions generated are lower than the ones from a blackbody at the same temperature [16]. The real rate of emissions can be expressed as:

$$\dot{Q}_{emit} = \varepsilon \sigma A_s T_s^4 \quad (2.11)$$

where ε is the emissivity of the surface. It has a value from 0 to 1 depending on the properties of the surface considered [16]. The emissivity for a blackbody is equal to 1, as in Equation (2.10). Another important parameter for radiation is the absorptivity α , which is the portion of the radiation energy that is absorbed by the surface. Both ε and α depend on the temperature and on the wavelength of the radiation.

2.3 Turbulence Modeling

Turbulent flows have always been important as they represent the real physics of many systems in reality and they have many peculiar characteristics. A very good definition comes from Hinze which states [15]:

"Turbulent fluid motion is an irregular condition of flow in which the various quantities show a random variation with time and space coordinates, so that statistically distinct average values can be discerned."

From this definition, it can be understood that turbulence implies a wide range of scales due to its irregular nature. Energy is exchanged among the eddies that are generated and it is transferred from the bigger to the smaller scales, in which it is dissipated [12]. Turbulence is present in a huge variety of engineering applications, and this is due to the fact that thanks to its characteristics, turbulence enhances the transfer of mass, momentum and energy to a great extent. This enhanced diffusivity can be several orders of magnitude bigger than that of a

laminar flow. Thus, in engineering practice this property is often used. For engineering simulations, it is too demanding to resolve all these scales due to their variety and characteristics. This applies to both the time the simulation will take to be completed and the computational demand it would require. For these reasons many ways have been studied to try to reduce the computational demand. One method that is used in common practice was introduced by Reynolds and it is the statistical averaging.

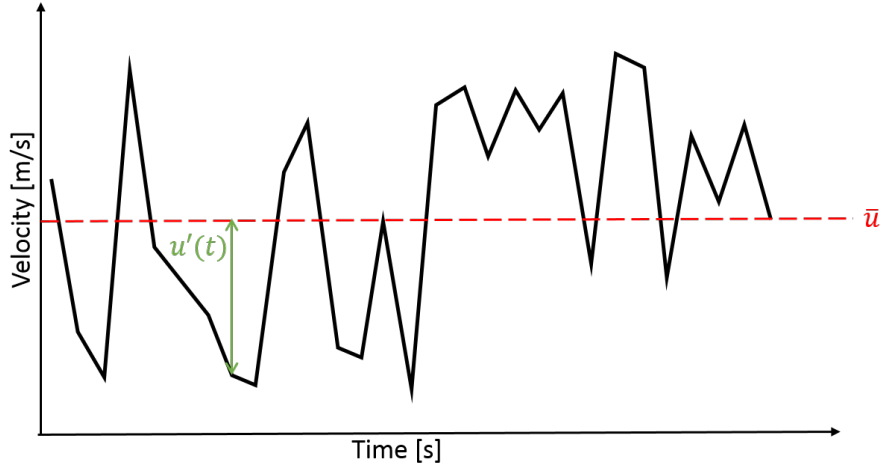


Figure 2.1: Velocity decomposition

In Figure 2.1, velocity is shown over time and space for a point in a turbulent flow. Any instantaneous velocity at a particular position in space and time, $u_i(x, t)$, can be expressed as the sum of two parts. One is the average velocity, \bar{u} or $\langle u \rangle$, and the second is the fluctuation part, u' , which varies over time and represents the turbulence [11]. This decomposition can be done for every fluctuating variable. In mathematical terms this is expressed for velocity and pressure as described in Equation (2.12) and (2.13). An important property of Reynolds-averaging is that it is always true that $\overline{u'} = 0$.

$$u_i = \langle u_i \rangle + u'_i = U_i + u'_i \quad (2.12)$$

$$p = \langle p \rangle + p' = P + p' \quad (2.13)$$

The time-averaged mean of a quantity $\phi(x_i, t)$ can be expressed as:

$$\langle \phi(x_i, t) \rangle = \frac{1}{2T} \int_{-T}^T \phi(x_i, t) dt \quad (2.14)$$

where the timescale T is larger than the turbulent time scales but smaller than the mean components' time scales [11]. This time averaging is usually useful and commonly used for incompressible fluids. When considering compressible fluids, density fluctuations must be taken into account along with velocity and pressure ones. If the time averaging method described below is used, additional modeling is required to achieve closure of unknown correlations [12]. This problem can be substantially simplified by using a mass-averaged statistical averaging, also known as Favre averaging. This averaging divides instantaneous variables such as velocity into two parts as follows:

$$u_i = \tilde{u}_i + u''_i \quad (2.15)$$

where \tilde{u}_i is the mass-averaged part and u_i'' the fluctuation one. Moreover, for Favre average it is always valid that $\overline{\rho u_i''} = 0$. This simplifies to a great extent the turbulent modeling equations. A Favre-averaged variable $\phi(x_i, t)$ can be expressed as:

$$\tilde{\phi}(x_i, t) = \frac{1}{2 \langle \rho \rangle T} \int_{-T}^T \rho(x_i, t) \phi(x_i, t) dt \quad (2.16)$$

2.3.1 RANS and FANS

By time-averaging over a reasonable time span, the fluctuations derived from turbulence can be separated from the non-turbulent quantities. Proceeding with this method, it is possible to obtain a set of equations called Reynolds Averaged Navier-Stokes equations, or RANS [11]. For incompressible flows they can be expressed as:

$$\frac{\partial U_i}{\partial x_i} = 0 \quad (2.17)$$

$$\frac{\partial U_i}{\partial t} + U_j \frac{\partial U_i}{\partial x_j} = \frac{\partial}{\partial x_j} \left(-\frac{P}{\rho} \delta_{ij} + 2\nu \bar{S}_{ij} - \overline{u_i' u_j'} \right) \quad (2.18)$$

where δ_{ij} is the kronecker delta function and \bar{S}_{ij} is the mean strain tensor, which can be expressed as:

$$\bar{S}_{ij} = \frac{1}{2} \left(\frac{\partial U_i}{\partial x_j} + \frac{\partial U_j}{\partial x_i} \right) \quad (2.19)$$

In equation (2.18), $-\overline{u_i' u_j'}$ is called Reynolds stress. As the mean of the product of fluctuations is not known, this non-linear term needs to be modelled to solve RANS equations. Favre-averaging can be used as well and it is usually done for variables that form a product with density to use the fundamental property of Favre averaging that $\overline{\rho \phi_i''} = 0$. The equations obtained are called Favre Averaged Navier-Stokes equations, or FANS. These, for a compressible fluid, can be written as:

$$\frac{\partial \bar{\rho}}{\partial t} + \frac{\partial}{\partial x_i} (\bar{\rho} \tilde{u}_i) = 0 \quad (2.20)$$

$$\frac{\partial}{\partial t} (\bar{\rho} \tilde{u}_i) + \frac{\partial}{\partial x_j} \left(\bar{\rho} \tilde{u}_i \tilde{u}_j + P \delta_{ij} + \overline{\rho u_i'' u_j''} - \bar{\tau}_{ij} \right) = 0 \quad (2.21)$$

Both these averaging methods can be applied analogously for the energy equation (2.5). Favre averaging can be useful for the specific total energy e since it is present in a product with density.

2.3.2 Realizable $k - \varepsilon$ Model

The non-linear terms in RANS need to be modeled to close the equations and to be able to solve them for each cell in the computational domain. Thus, it is necessary to implement some turbulence models to predict terms such as Reynolds stresses. The various models formulated are classified considering the number of additional transport equations that they require [13].

The most common type of turbulence models are the two-equation models. They are defined as complete models due to the fact that they allow both turbulent velocity and length scales to be calculated independently thanks to the introduction of two new transport equations of two selected variables [11]. As a consequence, these models can be used to predict the characteristics of a turbulent flow without having any prior knowledge about the turbulent structure of it [12]. Moreover, this type of turbulence models usually provides a good trade off between precision of results and computational demand and time used to complete the simulation. A type of two equation model is $k - \varepsilon$ and it is characterized by the addition of transport equations of the turbulent kinetic energy k and the energy dissipation rate ε . This model is widely used due to its robustness. However, the standard model fails to accurately predict flows that are not close to isotropic conditions, such as swirling flows, streamline curvature and axisymmetric jets. This stems from the fact that the model is based on the Boussinesq approximation, that assumes isotropy [11]. Models based on the Boussinesq approximation introduce the concept of eddy turbulent viscosity ν_T , which is determined through the additional equations provided. This eddy viscosity is used to solve the Reynolds stress tensor according to equation (2.22) below.

$$-\overline{u'_i u'_j} = -\nu_T \left(\frac{\partial U_i}{\partial x_j} + \frac{\partial U_j}{\partial x_i} \right) + \frac{2}{3} \delta_{ij} k \quad \text{where} \quad \nu_T = C_\mu \frac{k^2}{\varepsilon} \quad (2.22)$$

As a consequence of the problems described above, modifications of the standard $k - \varepsilon$ model have been introduced. One of them, which is of particular relevance for the project, is the Realizable $k - \varepsilon$ model. In it, C_μ is not constant anymore and it varies to keep normal stresses positive in any flow conditions, thus avoiding the violation of Schwarz's inequality [11]. In this way, flows that involve separation and rotation, such as swirling flows and planar/axisymmetric jets, are better predicted. Along with the variation of C_μ , this model also involves a modification of the ε -equation that has an additional production term.

2.4 Discretization Schemes

The basic principle behind the finite volume method is local conservation. The entire domain is divided into sub-volumes, called cells, for each of which the partial differential equations are solved [13]. To solve the equations, they have to be discretized for each cell. This is done employing Gauss' law, which rewrites volume integrals of a general quantity ϕ_i as surface ones according to:

$$\int_{CV} \frac{\partial \phi_i}{\partial x_i} dV = \int_{CS} \phi_i n_i dS \quad (2.23)$$

In this way the problematic transport equations can be expressed as a set of linear algebraic equations instead of partial differential equations [11].

Therefore, equations can be solved in a easier way for each cell, at the expenses of introducing an error in the solution. For example, the convection term can be expressed as:

$$\int_{CV} \rho \frac{\partial (U_j \phi)}{\partial x_j} dV = \int_{CS} \rho U_j n_j \phi dA_j \quad (2.24)$$

In Equation (2.24), CS denotes the control volume surfaces. Thus, the discretization method introduces the necessity of predicting quantities at the boundary surfaces of the cells.

Different discretization schemes can be used for this purpose. Two important properties for discretization schemes are *boundedness* and *transportiveness*. A variable is defined bounded if it has a value that is neither bigger or smaller than the values used to calculate it. Transportiveness can be defined as the capacity to sense in which direction the information is transported, thus taking into account for the direction of the flow. Upwind schemes are used in cases in which a strong convection is present. They are particularly useful in this type of situations because they make face values dependent only on upstream conditions [11]. Another important characteristic that these schemes have is that they take into account the direction of the flow, thus fulfilling the transportiveness property [13]. In the following subsections first order and second order upwind schemes are presented.

2.4.1 First order Upwind Scheme

The basic concept for the first order upwind scheme is to let the value of a shared face between two cells be equal to the value of the nearest upstream cell, which is found considering the flow direction. Thus, the first order upwind scheme is bounded and fulfills the transportiveness requirements. The major drawback associated with this scheme is that it is only first order accurate on the basis of the Taylor Series Truncation Error (TSTE) and this overestimates the entities' transport in the flow direction. This phenomenon is called *numerical diffusion* and it is more marked when the flow is not parallel to the cells [11].

2.4.2 Second order Upwind Scheme

The second order upwind scheme uses information from two upwind cells to predict the face values. This is done by assuming that the gradient between the cell considered and the western one is equal to the gradient of the eastern cell and the one considered. The second order upwind scheme is second order accurate on the basis of the TSTE, thus reducing the effects of numerical diffusion [11]. It still fulfills the requirements for transportiveness but it has the major drawback to be unbounded. This means that it could generate stability problems and unbounded results under certain flow conditions.

2.5 Cooling System

The cooling system of a car is of vital importance and ensures that the engine is operating at its optimum conditions. To get an efficient cooling system, the heat exchange between the incoming airflow and the system's components has to be studied and optimized. This can be problematic since the heat transfer includes complex boundary conditions and the coupling between air and solids [8]. To avoid excessive costs associated with late changes it is common practice to use CFD methods to optimize the cooling system in the early stages of the development of a car [14]. A simplified representation of a possible configuration of a car's cooling system can be seen in Figure 2.2. The parts more relevant for this project are explained below.

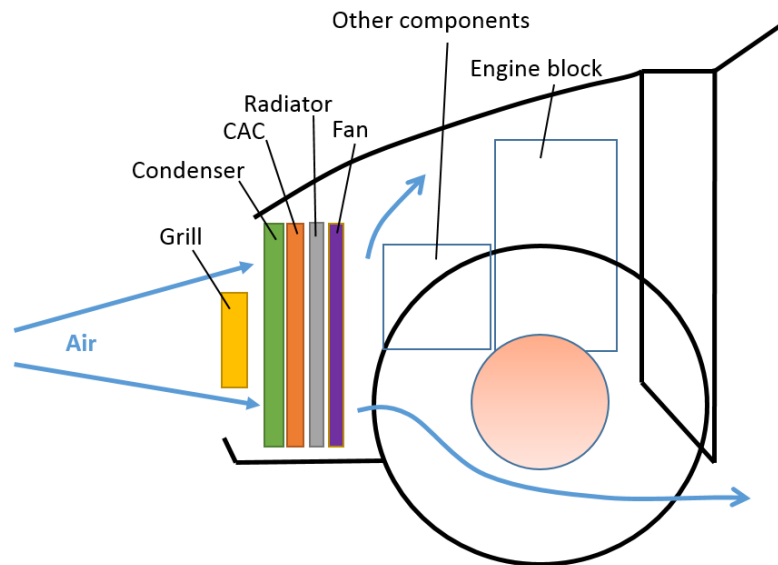


Figure 2.2: Main parts in a car's cooling system

2.5.1 Condenser

The condenser is a very important part of a car's cooling system. It is responsible for the heat exchange between the incoming air flow and the AC system's refrigerant, and it enables maintaining the interior temperature of the car at a satisfying level.

2.5.2 Charge Air Cooler

In modern engines, a new component added is the turbocharger, that is responsible for compressing air so that its amount in the cylinder is higher, allowing higher power output and lower fuel consumption. As a result of this compression, air's temperature increases as well. Therefore, the presence of the Charge Air Cooler (CAC) in the car's cooling system is of great importance, as it has the role of cooling the air before it enters the cylinder. This leads to reduced risks related to higher air temperature, such as early engine ignition and too high temperatures for the components to withstand.

2.5.3 Radiator

In a car, it is important to have a refrigerant ensuring that the engine block is continuously cooled to avoid serious damage to the engine. Usually the refrigerant consists of a mixture of water and glycol and it travels around the engine block, where it is heated. In the radiator the hot refrigerant's heat is dissipated and it is dispersed into the surrounding air. The heat is transferred from the refrigerant to the tube walls by convection, through walls by conduction and from walls to air by convection.

2.5.4 Fan

In the cooling system of a car there is always the presence of one or more fans. The fan increases the air flow through the heat exchangers. It is of vital importance, especially at lower speed conditions. The fan is always mounted behind the radiator.

2.6 MRF Fan Modeling

Obtaining an appropriate model of the fan is very important to predict the efficiency of the cooling system. In particular, an appropriate model should be able to predict the fan's influence on the flow since it influences both the heat exchangers and the rest of the underhood components. Over the years, many methods have been developed to reach this aim, involving different amounts of computational time demands and experimental data needed. Among them, the Multiple Reference Frame (MRF) approach is often used and it will be implemented in this project as well. It is a quite robust and simple method and it can often predict realistically the swirling flow components and pressure jump without the need for experimental data [1]. The basic assumption is that the volume assigned rotates at constant speed and that the surfaces of revolution are the non-wall boundaries [18]. As a result, running a simulation with this method allows to observe results of the rotating parts at the instant that corresponds to the position of the rotating part within the MRF. In order to use it, the Navier-Stokes equations include two extra acceleration terms, which represent the Coriolis and centripetal accelerations [17]. One of the major limitations of this method is that it is highly dependent of the choice of the frozen and rotating regions. This can affect the accuracy of the results obtained. Thus, a lot of effort has to be invested in a model to predict accurate results. In this project, the MRF model was previously set.

2.7 Porous Media Modeling for Heat Exchangers

In the cooling system considered, three types of heat exchangers (HXC) can be identified: the condenser, the radiator and the CAC. STAR CCM+ offers the use of different methods to simulate these regions, such as single or dual stream heat exchanger models and porous model. Since it is not important for the scope of the project to resolve the flow inside the heat exchangers, to capture the macroscopic effects of these geometries, they are often represented as empty cuboids. Then, they are modeled as porous regions in STAR CCM+. By modelling the heat exchangers in this way, major features are taken into account such as pressure drops and flow resistance. However, to be able to take into account the heat exchange there is the need of an additional model. For a segregated flow model to get a description of the macroscopic effects, STAR CCM+ includes additional source terms in the momentum equation for convection and viscous fluxes [19].

$$s_{p,i} = -P_{ij}^V u_j + P_{ij}^I |u| u_j \quad (2.25)$$

where P_{ij}^V and P_{ij}^I are the porous viscous and inertial resistances respectively. When there is heat transport across the porous regions, the thermal properties of the material have to be defined, such as solid density, specific heat and thermal conductivity [19].

2.8 Geometry Definition and Meshing

To get realistic results, it is important to have defined a proper geometry. In this case two geometries were combined, one more simplified and one more detailed. It was important to identify which parts are more important to be accurately resolved and give a smaller mesh cell size to those, leaving a larger size for parts that are not the focus of the analysis. This distinction has to be made to find a proper number of cells in the computational domain so that the time demand is reasonable, given the project time limit. Computer Aided Engineering (CAE) softwares like ANSA can be used to define and modify the geometry and clean it up.

2.8.1 Clean-Up of the Geometry

Geometry clean-up is an important pre-processing step. As a matter of fact, defining an acceptable geometry is the basis to obtain a proper mesh and realistic simulation results. It is used to fix imperfections that can be present in the initial geometry, such as disconnected edges, non-manifold and intersecting surfaces, gaps and excessive details. Surface wrapping algorithms are also possible methods used for geometry clean-up.

2.8.2 Volume Meshing

Meshing the volume considered for the simulation is a complex procedure that can be handled by different softwares. In this project, it was accomplished in STAR CCM+. In general, grids can be divided into structured and unstructured grids. The main difference is that the structured grids are generated from only hexahedral elements in 3D. This restriction makes the meshing faster, with better numerical properties and occupying less memory [11]. Moreover, it is easier to find neighbouring cells and indexing them. On the contrary, unstructured grids are made up by different elements, such as tetrahedra, hexahedra, prisms and pyramid elements. When handling complex geometries, it is impossible to mesh them using structured mesh. In STAR CCM+, the volume meshing is performed through the *Automated Mesh* option. This option has the benefit of enabling various type of volume meshing with different parameters and settings for the parts of the geometry. Thus, for each operation the parts to include can be selected along with the settings.

2.9 Steady State and Transient Simulations

During the project, different types of simulations were run, namely Steady State, Transient and Semi-Transient. In this section, the former two types will be presented as they have a more well established base. The Semi-Transient method will be presented in Chapter 3 as it is more a concept developed throughout the project than a established one. Steady State and Transient simulations differ mainly in the time dependence they involve. Steady state simulations are used when the aim is to get results about quantities at an equilibrium state, which is reached after a relatively long time [21]. They do not require real time information and are used usually when only the final status of a turbulent flow has to be investigated. When it is of interest to study the evolution of a flow over time, transient simulations are the best option as they show the development of the desired quantities over time [21].

2.9.1 Solution Methodology

The solution methodology that STAR CCM+ uses to solve SS and transient simulations can be seen in Figure 2.3. The Steady State solution methodology is represented by the inner loop, in yellow. The simulation runs until the equations are converged. Once the inner loop is solved, the simulation is finished. Transient solution methodology is represented by both the inner and outer loop, in yellow and light blue in Figure 2.3 respectively. In the inner loop, equations are solved for a specified physical time interval. For each inner loop, the number of inner iterations and the physical time interval can be set by the user. The outer loop relates the overall physical time we want the simulation to be run. Basically, for each inner loop the simulation advances for the specified time interval in physical time, until it reaches the stopping physical time by adding up the inner loop intervals.

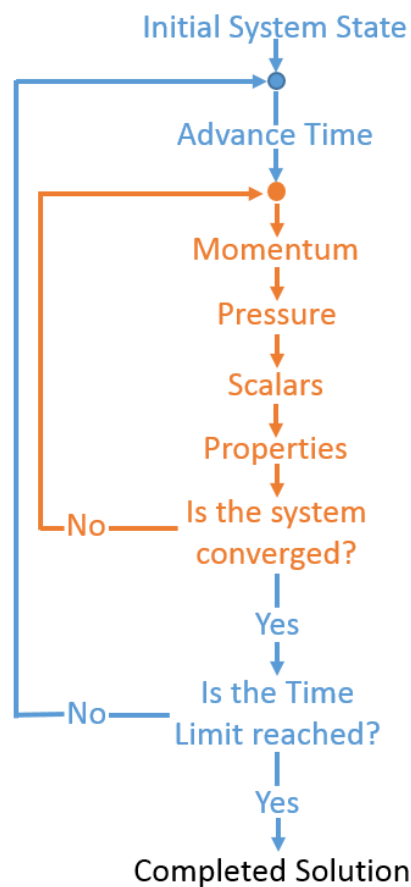


Figure 2.3: Solution methodology in STAR CCM+: outer and inner loops

2.9.2 Residuals

Residuals are an important parameter used to check convergence of a simulation. The conservation equations, such as energy, mass and momentum, are based on the assumption that the total flux of a conserved quantity at the inlet of an arbitrary volume is equal to the one at the outlet. When the volume is discretized in computational cells, this statement is not always correct. The differences between the inlet and outlet quantities' values are called

residuals [20]. Residuals can be used to keep track on how the solver is running and they should decrease during the overall simulation time.

For SS simulations, one way to check convergence is by observing if residuals are decreasing overall. It is also important to check the convergence of engineering quantities considered, keeping in mind that many times at convergence a variable oscillates between a range of values more than stabilizing at a single value [20].

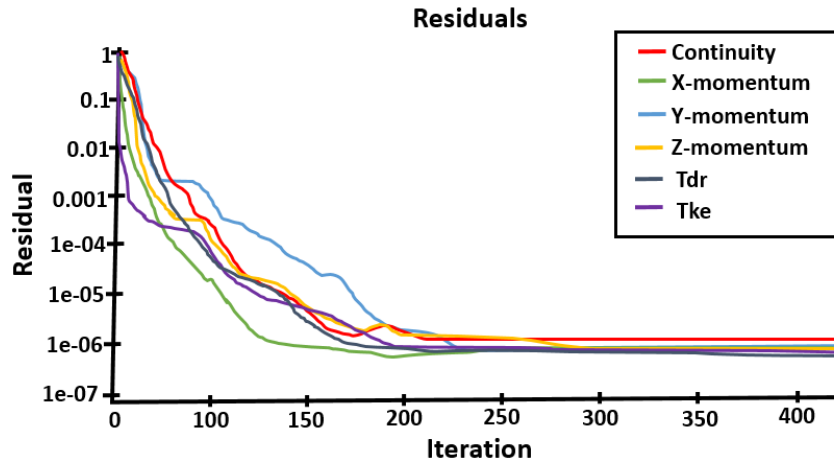


Figure 2.4: Typical residuals plot for SS simulations

Figure 2.4 shows a typical residuals plot for SS simulations. As it is possible to see, residuals decreased over time reaching a quite constant value after approximately 250 iterations.

For transient simulations, a typical residuals plot looks similar to the one for SS simulations for each time step. An example is shown in Figure 2.5.

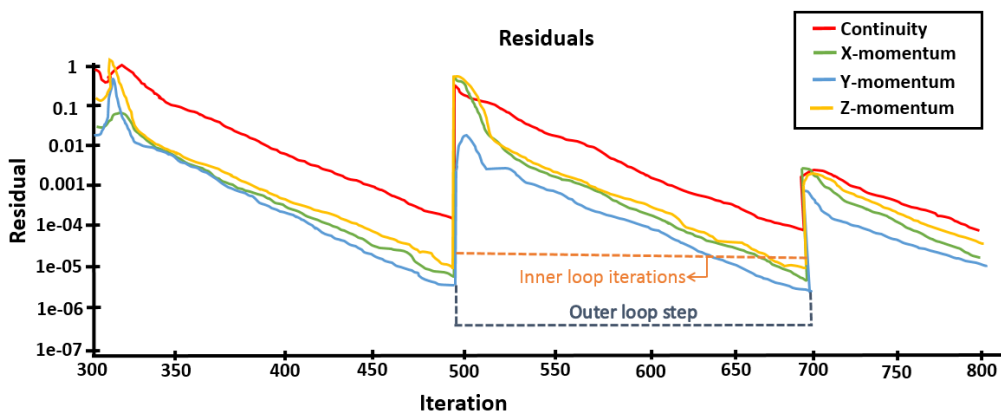


Figure 2.5: Typical residuals plot for transient simulations

In this plot it is possible to identify the two loops described in Figure 2.3 before. Basically, for each time step convergence is reached in the inner loop which iterates the solution, producing a plot similar to the SS one. Then the converged values for the cells are used as initial values

for the next time step [20]. Two important parameters to set in STAR CCM+ for transient simulations are *Time-Step* and *Maximum Inner Iterations*. The Time-Step defines the physical time that is simulated for each inner loop. Choosing an appropriate value for this parameter is essential for effective transient simulations. If it is too small, there is the risk of ending the inner loop before convergence is reached, introducing system errors which will add up during the simulation producing unreliable results. On the other hand, if the value is too high, it is likely that the solver reaches convergence before the inner loop is finished, wasting precious computational time [20]. The Maximum Inner Iterations criterion is relevant as well and can be used to prevent iterating indefinitely until the solver realizes convergence is reached, making the solver advancing after a defined number of iterations. The relevance of the two criteria described above can be seen in Figure 2.6.

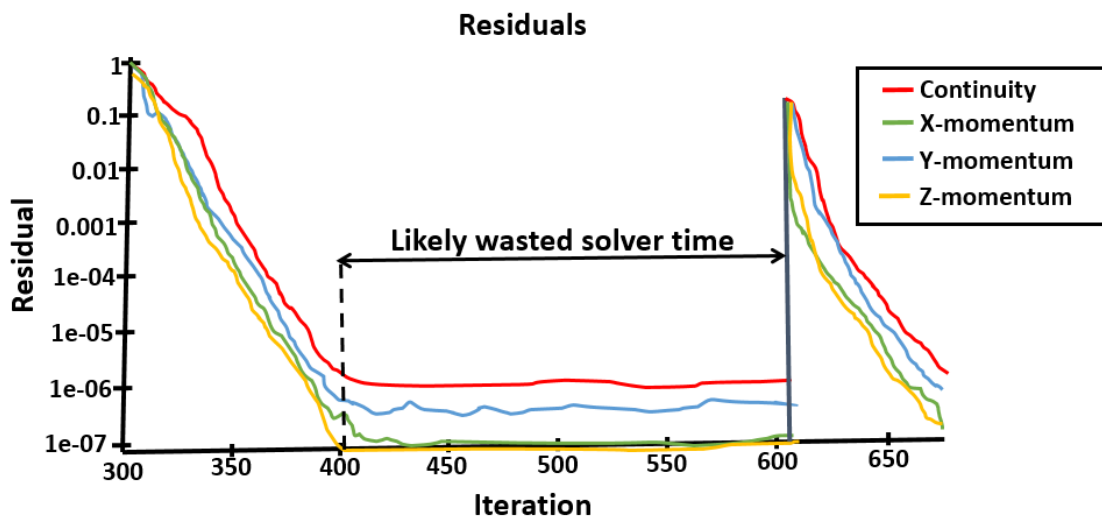


Figure 2.6: Example of the importance of setting optimized Time-Step and Maximum Inner Iterations Criteria

In the example in Figure 2.6, too conservative values for Time-Step and Maximum Inner Iterations were chosen. As a result, the solver reaches convergence long before the inner loop is completed and precious simulation time, shown in black, is wasted [20]. It is thus important to optimize the choice of values for these parameters since they are fundamental for the total simulation time and accuracy of results. This will be the underlying concept on which the Semi-Transient method will be defined.

3

Methods

This chapter has the aim of describing the main procedures and methods used for the simulation process. In the project, the geometry preparation was performed in ANSA while the meshing was accomplished through STAR CCM+ software. First, these two softwares will be discussed and presented. Then pre-processing techniques such as surface wrapping and remeshing will be presented. The settings definition for the simulations such as boundary and initial conditions are discussed as well. Finally, solver settings and the Semi-Transient method will be presented.

3.1 Software used

The two main softwares used for this project are ANSA and STAR CCM+. These are described below.

3.1.1 ANSA

ANSA 17.1.2 from BETA CAE Systems S.A. provides a series of powerful tools to create, manipulate and improve a geometry. This software offers a wide range of pre-processing techniques to clean-up a geometry, prepare it for meshing and accomplish an initial mesh. If the tools are properly used, the work on the next processing tools such as STAR CCM+ is then consistently simplified. ANSA's tools can aim at different degrees of detail. As an example, the surface wrapping can be accomplished with constant length, as a fast and economic way, or with variable length, to capture the small details of the geometry.

3.1.2 STAR CCM+

STAR CCM+ is defined by Siemens as "*a complete multidisciplinary platform for the simulation of products and designs operating under real-world conditions*". It provides a wide range of tools that cover the simulation of a huge variety of physical phenomena that are needed to be simulated together in order to get realistic results. Moreover, it is designed to allow changes to be applied relatively fast. For example, operations such as surface wrapping and automated mesh are ordered in a specific sequence in a pipeline. This allows per-part meshing. The major benefit of it is that when a modification is made it is not necessary to run all the operations again. Instead STAR CCM+ identifies the operations that need to be changed without changing the others, thus saving a lot of time. Moreover, the program is supported by an active group of experts that help users to solve problems and understand better how the software works.

3.2 Geometry Preparation

To reach the aim of the thesis, it was necessary to define an appropriate geometry of the car and the underhood compartment to simulate and develop a simulation system to model it, focusing on the thermal profiles in the underhood compartment. The starting model was a simplified geometry made by Randi Franzke, CFD driven analysis engineer at Volvo Cars. This will be called from now on *start geometry* and it is shown in Figure 3.1.

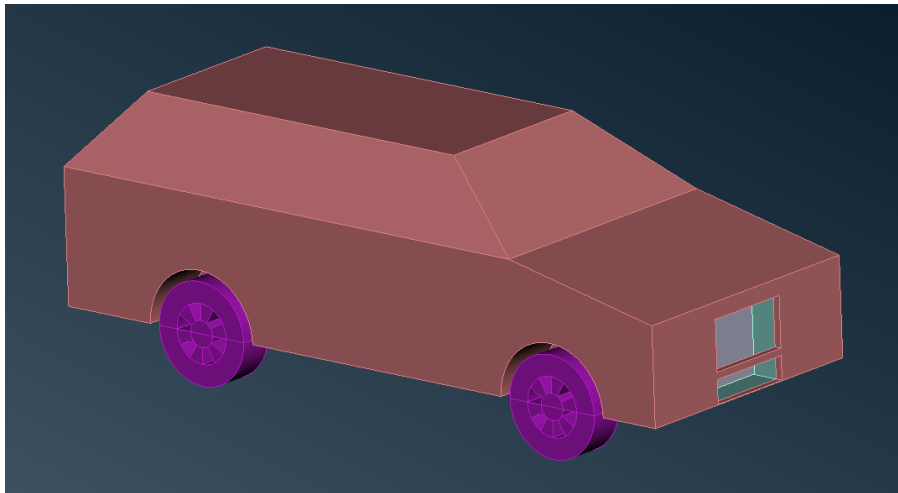


Figure 3.1: Entire simplified car

The simplified geometry is a car in a wind tunnel. The simplified underhood compartment was analyzed to understand if the simplifications in the geometry were too limiting. The initial simplified underhood compartment can be seen below.

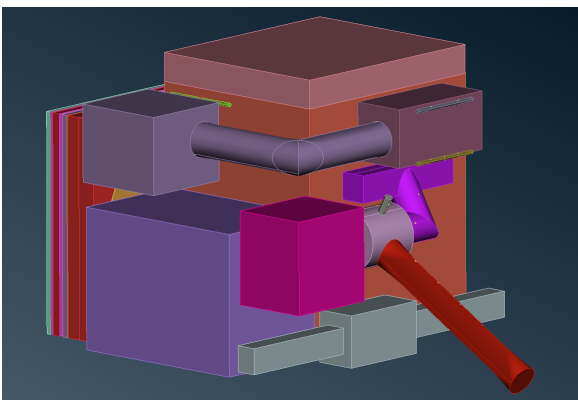


Figure 3.2: Simplified underhood compartment

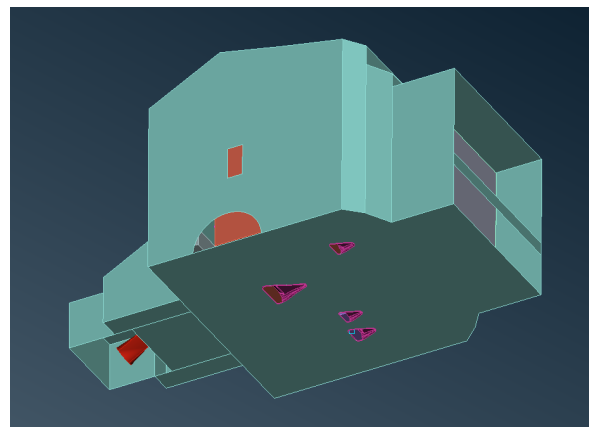


Figure 3.3: Engine bay and openings

In Figure 3.2 the different parts of the underhood compartment are shown. On the bottom left side, corresponding to the front of the car, the condenser, heat exchanger, radiator and fan can be seen in series. They have been substituted as empty cuboids that will be modelled as porous regions. The engine with its cover is shown as an orange box. It will be considered isothermal assuming that the coolant will keep it around the same temperature. Other three adiabatic

boxes are placed to fill up empty spaces which are not present in car engines and the gear box is represented by the purple box on the left side. The remaining parts represent the manifold to which the catalyst for the exhaust gas aftertreatment system is connected along with the exhaust pipe. In Figure 3.3 the engine bay is shown along with its openings. In particular, it is possible to observe that underbody openings are present to let the fresh air come in while the car is driven. Their effect is more pronounced thanks to the uphill position of the car which allows more fresh air to enter giving an extra forced convective cooling [2]. Also, the exhaust pipe is simplified and exits from the car in the middle, and not in the rear. After an accurate analysis of the start geometry, some parts have been chosen to be too simplified. These are the manifold, turbo and the exhaust aftertreatment system. The geometry for these parts was taken from a more detailed geometry, called from now on the *detailed geometry*. The next steps consisted in cleaning up both the start and the detailed geometry.

3.3 Geometry Clean-Up

Using ANSA as software, the clean-up of both the geometries could be accomplished. Then, they were combined to lower the resulting amount of computational cells but keeping details on more important parts. Where unnecessary holes were present, they were filled using the manual fill command and two layers were created in order to give to the surface some thickness for the next volume meshing, which was performed afterwards in STAR CCM+. The unnecessary parts were eliminated as well. Moreover, to simplify the model small surfaces were grouped together into bigger PIDs, which can be seen in different colour. As an example of geometry clean-up, the parts taken from the detailed geometry are shown before and after it in Figures 3.4 and 3.5 respectively.

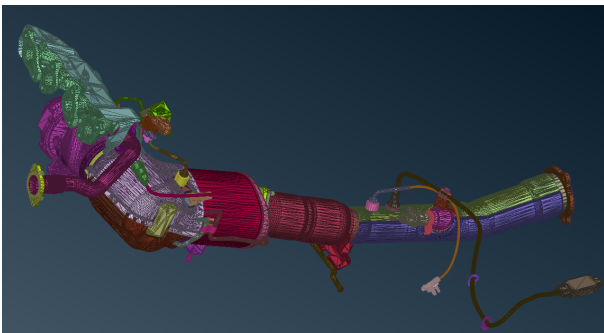


Figure 3.4: Detailed geometry before geometry clean-up

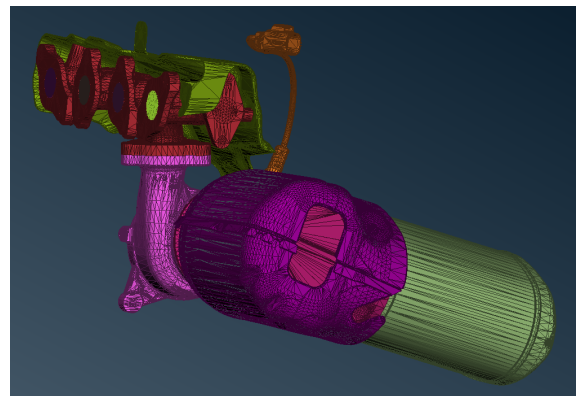


Figure 3.5: Detailed geometry after geometry clean-up

The manifold, shown in red, represents the entrance from which the exhaust gases are distributed. Above it, a heat shield is present as well, colored in green. This will have two metallic layers separated by an intermediate insulation layer. Below the manifold, the turbo compressor is present and then two different catalysts, together with their insulation and metallic layers are present as well. A sond, represented in orange, was kept. This modified geometry was introduced in the starting one to replace the parts which were considered too simplified and it was properly oriented to be introduced in the simplified geometry. Other

modifications that were made in the geometry included:

1. Some components that can be particularly sensitive to temperatures have been added. A simplified absorber was introduced in the the upper part of the engine bay. It was later divided into two to capture multiple hot spots present on the surface.
2. Rubber cylinders were moved in more critical spots of the engine. Three rubber cylinders are present in total with the following positions: between the exhaust system an one adiabatic box, between the exhaust system and the turbo, above the gear box.
3. The engine bay was modified to try to reduce as much voids. This was done for two main purpose. One was to reduce the number of computational cells, the second was to reproduce as much as possible the reality of the engine, which is very crammed.
4. The exhaust gas pipe was not replaced but just eliminated and the geometry was changed so that the outlet gases are directed towards the outlet at the bottom of the car.
5. The heat shield present in the model did not have an insulation mat. Thus, this was created to get more realistic results. For this purpose the Extraction operation in STAR CCM+ was very helpful to extract the volume between the heat shield and the insulation layer, which then corresponds to the two external metallic layers of the heat shield.

The resulting geometry is shown in Figures 3.6 and 3.7.

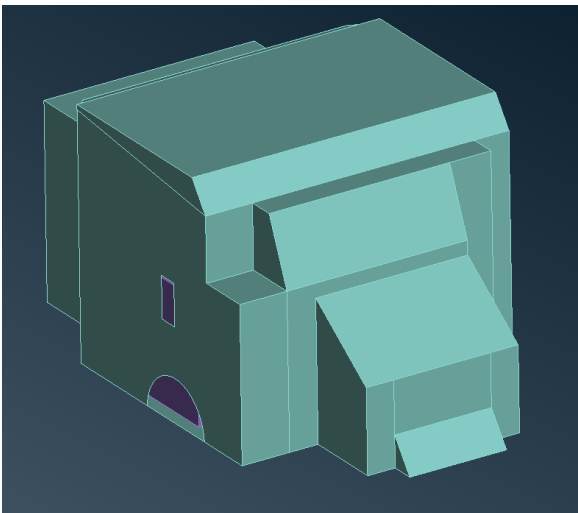


Figure 3.6: Modified engine bay

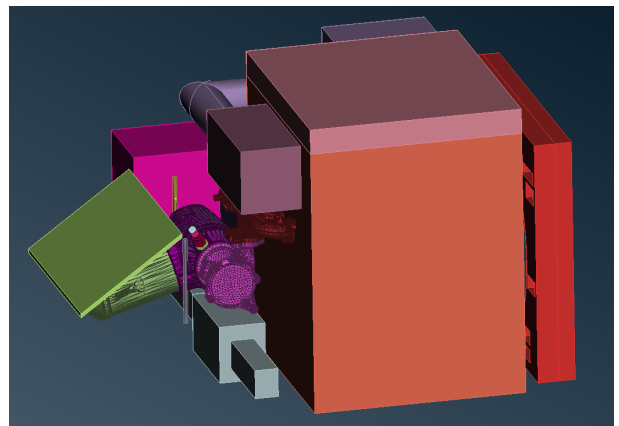


Figure 3.7: Final elements inside engine bay

3.4 Volume Meshing

Once the geometry is appropriately prepared, the next step is to volume mesh the desired domain to be able to run the simulation. The domain consists of a car in a wind tunnel. The wind tunnel has a size of 49.85x9.40x9.85 m, while the car's maximum dimensions are 5.00x1.92x1.45 m. Figures of the computational domain can be seen in Appendix A.1. Regions had to be defined as well, since each part has to be assigned to a region in order to be volume meshed. For each region it is important to define the parts included, the type of region and

the physics continuum associated with it. Table 3.1 presents the different regions used in the model and their main characteristics.

Table 3.1: Regions description

Region name	Type	Physics Continuum
First catalyst stone	Porous	Exhaust flow
Condenser	Porous	Physics Air
Exhaust gas flow	Fluid	Exhaust flow
Second monolith stone	Porous	Exhaust flow
Radiator	Porous	Physics Air
Solids	Solid	Physics Solid
Surface Wrapper Air side	Fluid	Physics Air
Surface Wrapper Fan	Fluid	Physics Air
Wcac	Porous	Physics Air

For this project it was important to define a range for the target total number of computational cells to reach. This is due to the fact that the number of computational cells must be limited to a manageable number to allow simulations, especially the transient one, to be concluded in a reasonable amount of time. The volume meshing was accomplished in STAR CCM+ and it can be divided into different steps which are surface wrapping, surface remeshing and final volume meshing.

3.4.1 Surface Wrapping

A complex and articulated geometry as the one that is considered in this project can have many imperfections, such as intersecting faces and small gaps. To get rid of these, the surface wrapping operation can be used, which allows to obtain manifold surface representations. STAR CCM+ offers a more accurate surface wrapping operation with respect to the one ANSA does. For example it is possible to include also some refinements such as surface curvature and proximity, contact prevention and custom controls based on the desired cell size for different parts of the geometry. Thus, the surface wrapping for each region was performed in STAR CCM+ after the geometry was imported. This was done in each region and its quality highly affects the next steps of the meshing.

3.4.2 Surface Remeshing

Surface remeshing is an option that can be included in each *Automated Mesh* (AM) operation in STAR CCM+, where the volume meshing is performed. It has the aim to further improve the overall cell quality of the surface wrapping, which is the basis for the volume meshing. In this way the volume meshing could be improved. For all the automated mesh operations in this project, surface remeshing was used and curvature and proximity refinement have always been included. On the other hand, surface remeshing has the tendency of generating some intersecting faces when the geometry considered is complex. For this reason another command is often used together with surface remeshing, which is *Automatic Surface Repair* operation. This operation takes place in between surface remeshing and volume meshing operations.

3.4.3 Final Volume Meshing

After the steps described above, the final volume meshing can be performed. Depending on the region and its role in the car system, different types of meshers have been implemented. For the solids, polyhedral and thin meshers were used. For the exhaust and porous regions of the catalysts polyhedral and prism layer meshers were used. For the heat exchangers, the trimmed cell mesher was used and for the fan polyhedral, thin and prism layer meshers were used. Finally, trimmed cell and prism layer meshers were used for the fluid domain. Target and minimum surface sizes (referred to as TSS and MSS respectively) were defined as well as surface growth rate (SGR) and number of layers (NL). Table 3.2 shows these parameters for the different AM operations.

Table 3.2: Automated Mesh parameters

AM	TSS [mm]	MSS [mm]	SGR	NL
Solids	4	3	1.2	2
Exhaust and porous region	10	5	1.3	5
Heat Exchangers	4	3	1.3	-
Fan	4	3	1.3	2
Fluid domain	8	2	1.3	1

As in the Surface Wrapping operations, in the AM operations surface controls have been added. Surface controls on solids parts were used according to their desired cell size. In these controls, target surface size and minimum surface size were defined. Another surface control was applied for the non-solid parts, where the number of layers was controlled. Moreover, since the zones near and inside the car are of more interest, the domain was divided into 7 refinement blocks. These have been used to set Volumetric Controls (VC) in the AM of the Fluid Domain. Pictures of the various blocks are included in Appendix A.2.

Table 3.3 describes the different blocks, the VC in which they are used and the custom isotropic cell size assigned to them.

Table 3.3: Blocks and Volumetric Controls

Block name	VC name	Custom isotropic cell size [m]
Around car and wake	Around car and wake	0.2
Around rear	Around car	0.032
Around front	Around car	0.032
Around intake	Grill	0.016
Inside engine bay	Around engine	0.008
Around exhaust	Around exhaust	0.004
Around HXCs and Fan	Around engine	0.008

After a first simulation run, reverse flow was observed in the outlet of the exhaust gas. To avoid this phenomenon, a fictitious exhaust pipe was introduced at the end of the exhaust gas outlet to remove reverse flow. This has been wrapped and meshed together with the rest of the exhaust gas flow domain, but it is not considered in the fluid flow domain. The final mesh

consisted of around 7.9 million cells and can be seen in Figures 3.8, 3.9, 3.10, 3.11, 3.12 and 3.13. Pictures were taken from two main sections, one cutting the domain vertically and one horizontally. These sections will be called section 1 and 2 respectively. Moreover, colour coding is also used, in which each colour represents a different region that has been defined in the simulation file.

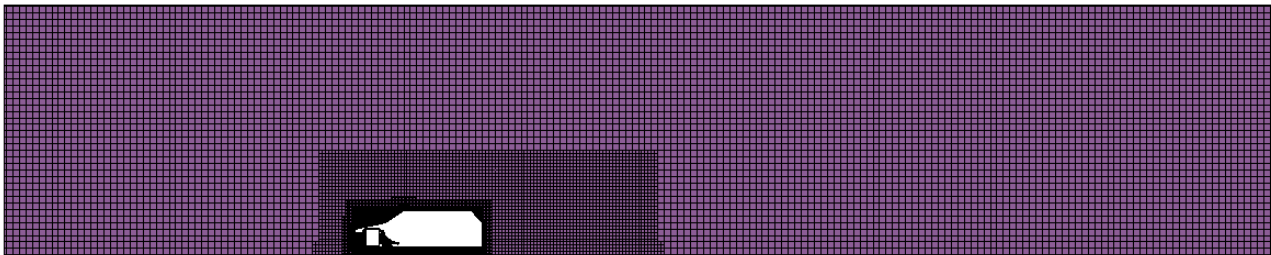


Figure 3.8: Overall domain, section 1

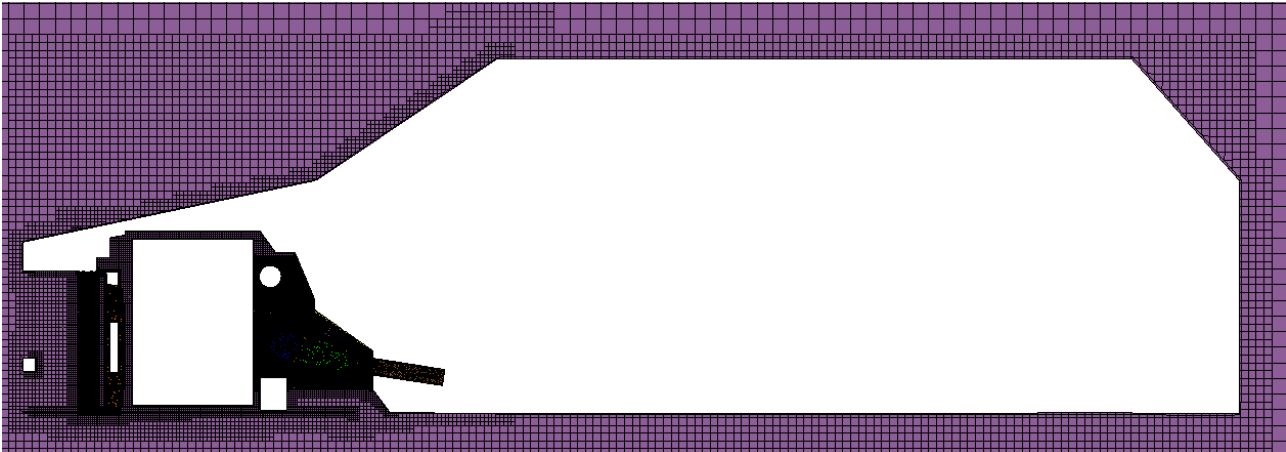


Figure 3.9: Car focus, section 1

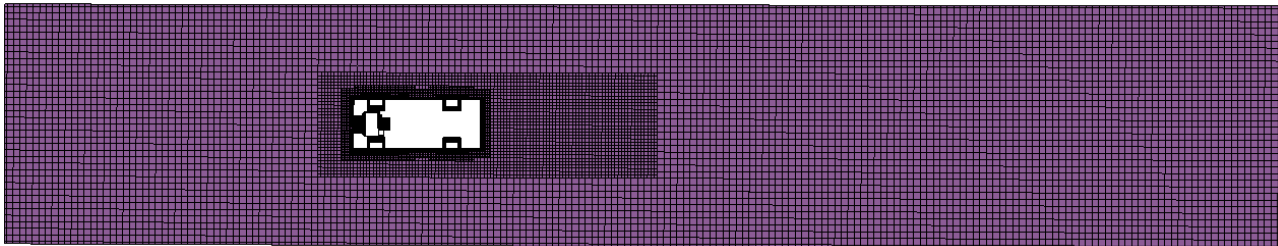


Figure 3.10: Overall domain, section 2

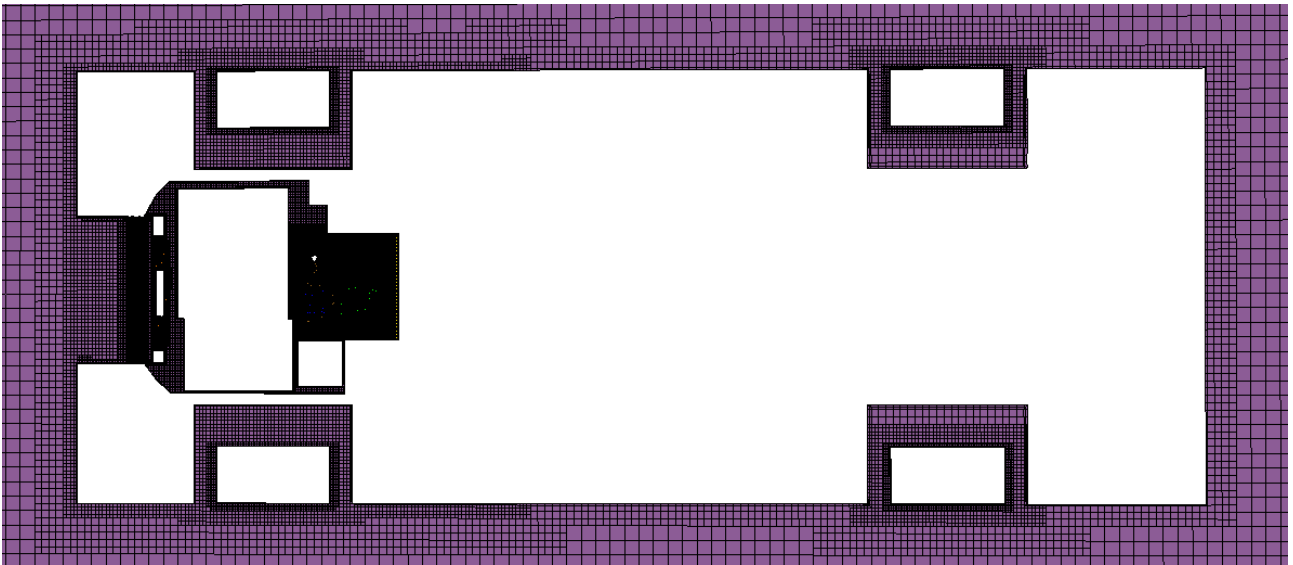


Figure 3.11: Car focus, section 2

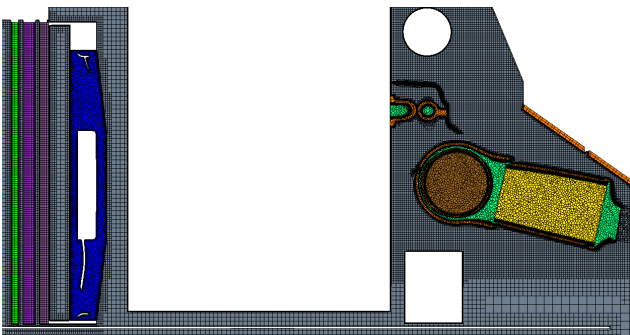


Figure 3.12: Underhood focus, section 1

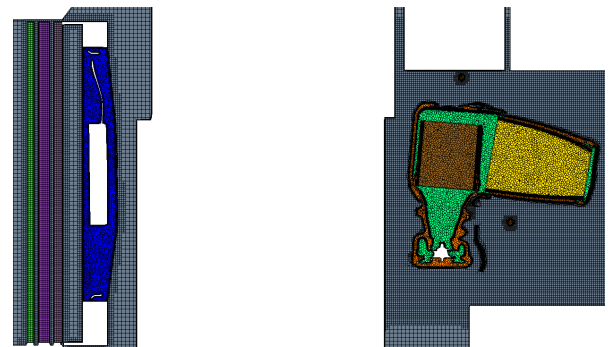


Figure 3.13: Underhood focus, section 2

3.5 Model Selection

When defining the simulation file, different continua had to be defined and appropriate models had to be chosen for each of them. Table 3.4 provides an overview of the different models selected for each continua. In addition to the list of models shown in Table 3.4, for each continuum either SS or Implicit Unsteady model had to be selected according to the type of simulation to be run. When selecting the Implicit Unsteady model, an appropriate time-step and maximum number of iterations per inner cycle had to be defined as well. Their values for this project will be explained in Section 3.7.2.

Table 3.4: Models for each continua

Exhaust Flow	Physics Air	Physics Solids
Cell Quality Remediation	Cell Quality Remediation	Cell Quality Remediation
Exact Wall Distance	Exact Wall Distance	Constant Density
Gas	Gas	Gradients
Gradients	Gradients	Multi-Component Solid
Gray Thermal Radiation	Gravity	Multi-Part Solid
Ideal Gas	Gray Thermal Radiation	Segregated Solid Energy
K-epsilon Turbulence	Ideal Gas	Three Dimensional
Radiation	K-epsilon Turbulence	
Realizable K-Epsilon Two-Layer	Radiation	
Reynolds-Averaged Navier-Stokes	Realizable K-Epsilon Two-Layer	
Segregated Flow	Reynolds-Averaged Navier-Stokes	
Segregated Fluid Temperature	Segregated Flow	
Surface-to-Surface Radiation	Segregated Fluid Temperature	
Three Dimensional	Surface-to-Surface Radiation	
Turbulent	Three Dimensional	
Two-Layer All y+ Wall Treatment	Turbulent	
View Factors Calculator	Two-Layer All y+ Wall Treatment	
	View Factors Calculator	

In the Solids Physics the Multi-Part solid model was selected. In this way it was possible to introduce different types of material in the system and assign the solid parts to each of them. Moreover, the *Allow Per-Part* option was enabled. In this way the solid parts were divided into different subgroups and it was possible to assign the appropriate emissivity value for each group at the interfaces between the solids and the air side and between the solids and the exhaust flow. Table 3.5 shows the list of materials, parts included and emissivity values used at the interfaces.

Table 3.5: Materials and emissivities list

Material	Parts included	Emissivity value
Absorbent	Lower and upper absorber	0.95
Ceramics	UHEGO ceramic part	0.45
Insulation elrotherm	Internal insulation for: first catalyst, second catalyst and heat shield	0.45
Plastic PA66 F35	UHEGO filter	0.95
Rubber EPDM	All rubber cylinders and rubber bushing of UHEGO	0.95
Stainless steel	Heat shield and	0.25
Aluminized 120	UHEGO metal cylinder at bush	0.45
Stainless steel ferritic	All other parts	0.45

3.6 Boundary Conditions

In the project, the three main simulation types are Steady State (SS), Transient (or Unsteady) and Semi-Transient. There are two main differences between these simulations. The first one regards the type of solver’s settings used. The different simulations and their solvers will be explained in Section 3.7. A second important difference between the simulations consists in using different Boundary Conditions (BC). Realistic estimates for them were taken for each phase from wind tunnel test results of a car driving at the investigated conditions. The program used to display the test results is Windows Forms Measurement Analysis. The case used to retrieve BC is the HCTR908.38.6.70 one, which has both the conditioning and the hill climbing with high load phases. An important observation to make is that the model of the car used in the project is simplified with respect to reality and thus it was important to understand which values and measurements could be used from tests.

Concerning the porous inertial and viscous resistances, they have been defined through the use of defined field functions for each porous zone. Particular attention was paid to the turbo. To improve the gas flow, when testing the model a turbo wheel was introduced without being rotated to save some computational time. The rotation of the turbo wheel is responsible for a decrease in exhaust flow temperature of about 100 °C. To take this effect into account, the BC for the inlet exhaust gas temperature was directly lowered by 100 °C with respect to test results.

Figure 3.14 describes the sequential steps taken through the project to obtain all the BC and simulations needed for comparison.

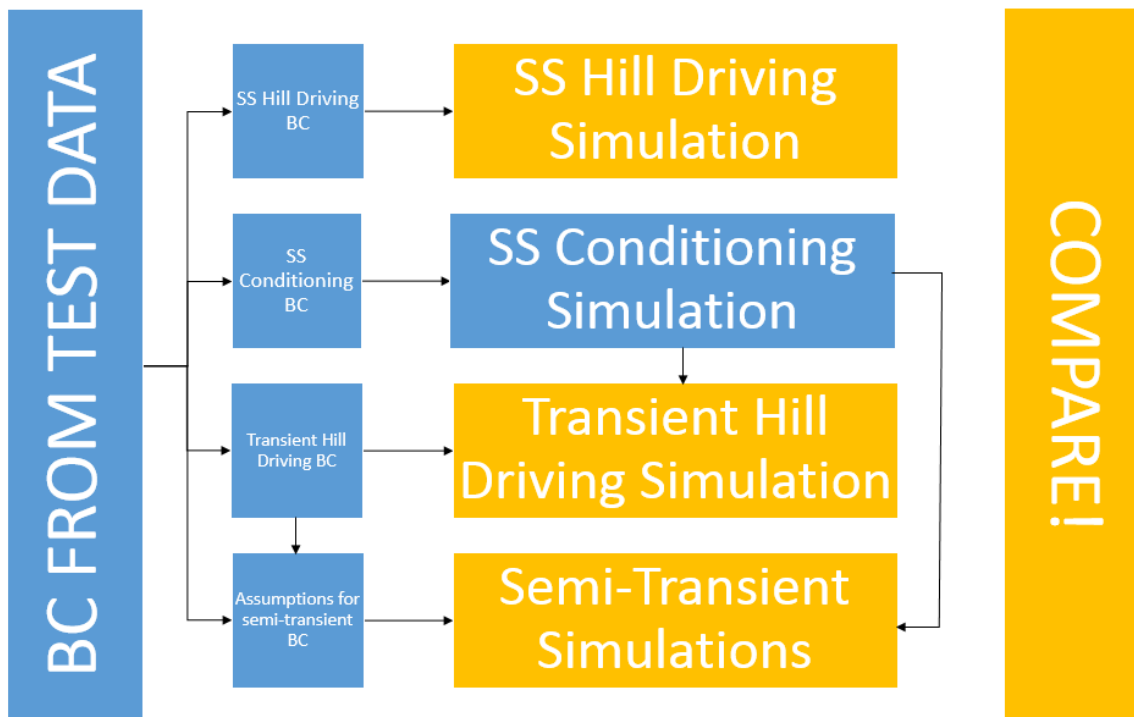


Figure 3.14: Methodology

As it is possible to see, different BC were taken for the SS hill driving and conditioning cases as well as for the transient hill driving case. By implementing the BC found in the simulation file, the SS conditioning and hill driving cases were run. The next step consisted in starting from the SS conditioning phase and changing the BC to transient hill driving conditions ones. Moreover, the solver had to be changed from steady to unsteady. In this way the Transient hill driving simulation was obtained. The SS and transient hill driving simulations were then kept to be used for comparison. The SS conditioning simulation was used another time as the starting file and semi-transient cases were run by changing the solver's parameters and using the same BC of the transient simulation. Finally these simulations were kept as well for comparison.

3.6.1 Steady-State Simulations

The various BC used for SS simulations in the project are shown in Table 3.6.

Table 3.6: SS Boundary Conditions

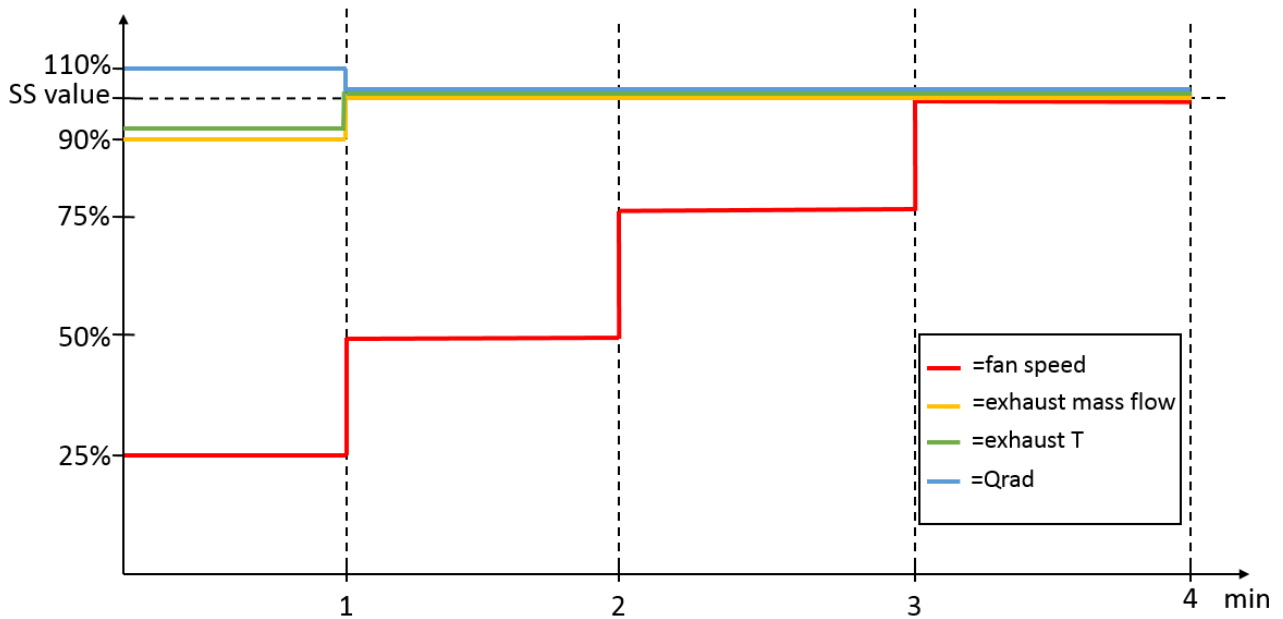
Region	SS Conditioning BC	SS Hill Climbing BC
Condenser	Total Heat Source = 5 kW No-slip wall condition	Total Heat Source = 5 kW No-slip wall condition
Exhaust Gas Flow	$\dot{m}_{in} = 0.021 \text{ kg/s}$ $T_{in} = 630^\circ\text{C}$ Pressure outlet	$\dot{m}_{in} = 0.065 \text{ kg/s}$ $T_{in} = 850^\circ\text{C}$ Pressure outlet
Radiator	HXC Option Inferred outlet T $\Delta T_{min} = 7 \text{ K}$ $Q = 15 \text{ kW}$ $T_{HXC} = 120^\circ\text{C}$ No-slip wall condition	HXC Option Inferred outlet T $\Delta T_{min} = 7 \text{ K}$ $Q = 44 \text{ kW}$ $T_{HXC} = 120^\circ\text{C}$ No-slip wall condition
SW Air side	$T_{engine} = 100^\circ\text{C}$ fixed $T_{windtunnel,in} = 27^\circ\text{C}$ $v_{windtunnel,in} = 70\text{kph}$ Pressure windtunnel outlet	$T_{engine} = 100^\circ\text{C}$ fixed $T_{windtunnel,in} = 27^\circ\text{C}$ $v_{windtunnel,in} = 70\text{kph}$ Pressure windtunnel outlet
WCAC	HXC Option Inferred outlet T $\Delta T_{min} = 10 \text{ K}$ $Q = 1 \text{ kW}$ $T_{HXC} = 100^\circ\text{C}$ No-slip wall condition	HXC Option Inferred outlet T $\Delta T_{min} = 10 \text{ K}$ $Q = 11.5 \text{ kW}$ $T_{HXC} = 100^\circ\text{C}$ No-slip wall condition

3.6.2 Transient and Semi-Transient Simulations

Both these types of simulations have been run using the Implicit Unsteady solver. In these cases, some BC were not set as constant anymore, but as scale functions whose value changed every minute in the first 4 minutes of physical time. The values at different minutes were taken as a percentage of the final SS value. This was done to better reproduce the system according to the test results observed. The BC over time are shown in Table 3.7 and Figure 3.15.

Table 3.7: Transient Boundary Conditions

	Minute 1	Minute 2	Minute 3	Minute 4
Fan Speed	25%	50%	75%	100 %
Exhaust inlet mass flow	90%	100%	100%	100%
Exhaust inlet T	-70 °C	$\pm 0^\circ\text{C}$	$\pm 0^\circ\text{C}$	$\pm 0^\circ\text{C}$
Radiator Heat Source	+10%	$\pm 0\%$	$\pm 0\%$	$\pm 0\%$

**Figure 3.15:** Transient and Semi-Transient Step BC

For reference later, the BC for the first four minutes will be referred to as Set 1, 2, 3 and 4 respectively. Please note that Set 4 will then coincide with the final BC settings for the remaining minutes of the simulations. Concerning the initial conditions, they have been set as continuum values.

3.7 Solver Settings

In general, it can be said that STAR CCM+ solver tries to satisfy the conservation equations starting from a set of BC, initial conditions and sources. As a result, velocity, pressure and temperature fields are updated for each cell in each iteration, until the discrete equations are satisfied [20]. This is an iterative process and its duration depends on the complexity of the system considered, the amount of cells, the BC and initial values and the models selected. Solver settings are different according to the type of simulation that is run and their choice highly influences the computational time required and the accuracy of results. A discussion of solver settings used for each case is provided below.

3.7.1 Steady-State Simulations

Solver settings for SS simulations are rather simpler than the ones for Transient and Semi-Transient ones. In particular, the choice of under-relaxation factors is important. Under-relaxation factors are used by the solver to simplify non-linear terms in the transport equations [11]. A generic under-relaxation factor α can be defined as:

$$\phi_{new} = \alpha\phi_{solver} + (1 - \alpha)\phi_{old} \quad (3.1)$$

Where ϕ_{new} is the new variable's cell value, ϕ_{solver} the one of the last iteration and ϕ_{old} the previous cell value used to calculate ϕ_{solver} . Each transport equation that is solved has its own under-relaxation factor, whose value is usually between 0 and 1. A value of α lower than one usually helps to get the simulation more stable, however a very low value will imply very little corrections and an increased simulation time which is undesirable [13]. It is also important to highlight that under-relaxation factors do not influence the final result of the simulation, but only the time needed to reach it [11]. In engineering practice, under-relaxation values are usually set lower at the beginning of the simulation and increased later. This was the approach used for the project's SS simulations. Table 3.8 shows the final values for under-relaxation factors.

Table 3.8: Final under-relaxation values

Under-relaxation factor	Final value
Segregated Flow Velocity	0.7
Segregated Flow Pressure	0.3
Fluid Segregated Energy	0.95
Solid Segregated Energy	0.99
K-epsilon Turbulence	0.6
K-epsilon Turbulent Viscosity	0.8

For what concerns the stopping criteria, a maximum number of iterations can be set, after which the simulation stops. In the SS simulations considered it was not possible to know a priori after how many iterations the solution would converge, thus this criterion was not enabled. Another stopping criterion that can be set relies on the residuals' values. In particular, it is possible to stop the simulation when selected residuals go below a limit value that can be arbitrarily set by the user. For the cases run in the project, none of these stopping criteria were used. Residuals and physical variables were manually monitored during the simulations run to decide when to stop them, according to guidelines explained in Section 2.9.2.

3.7.2 Reference Transient Simulation

For the reference transient simulation, maximum inner iterations and time-step are important parameters to set, for the reasons explained in Section 2.9.2. To get a first estimate of a time-step value, Courant number, or CFL, was used. CFL gives an indication of how the fluid is moving through the different computational cells and it can be defined as:

$$CFL = \frac{u\Delta t}{\Delta x} \quad (3.2)$$

Where u is a mean estimate of linear velocity, Δt is the time-step size and Δx is the characteristic cell length [20]. By reversing Equation 3.2, a first value of time-step can be calculated as:

$$\Delta t = \frac{\Delta x \cdot CFL}{u} \quad (3.3)$$

From 3.2, it is possible to conclude that CFL depends on velocity, time-step and cell size.

By observing CFL number, some considerations can be made. In particular, when $CFL \leq 1$, the fluid is likely to move from one cell to the next one within approximately one time-step. As a result, convergence and accuracy are improved, while numerical dispersion and oscillations are decreased. On the contrary, when $CFL \geq 1$, it is likely that fluid moves across two or more computational cells in one time-step. This may result in lower accuracy and difficult convergence. Thus, it is common practice to try to maintain CFL value at maximum 1.

For the case considered, it was difficult to get a realistic estimate of a time-step for many reasons. First, the system considered has many different cell sizes in different areas, as was explained in 3.4. Moreover, velocities cover a wide range of values as well, both for the air and exhaust gas continua. Using a conservative approach, the value of CFL should be set to 1, the velocity to the biggest value and cell size to the smallest value. However, it is important also to keep in mind that this will result in a very small time-step, which will significantly increase the computational time demand. For these reasons, a CFL number of 5 was chosen for the calculation in the case considered. Table 3.9 shows the values used for each variable and the resulting first tentative time-step obtained for the reference transient simulation.

Table 3.9: Calculation of first tentative Time-Step

Variable	Value
CFL	5
u	50 m/s
Δx	4 mm
First Tentative Time-Step	$\sim 1e - 4s$

After having identified a first tentative value for the time-step, this was used together with a maximum inner iterations number of 6. In order to find the optimal combination of these two factors, different plots of engineering quantities were studied and parameters were changed with the aim to increase as much as possible the time-step value without compromising the quality of the simulation solver.

After many tentatives, the solver was found to be very sensitive even to the slightest variation of the time-step value. At the end, the simulation's parameters were set with a time-step of $6e-5$ s and 4 maximum inner iterations. After 1.1 seconds the flow field seemed to be stabilized and a new attempt of increasing the time-step was tried. This resulted in a new increased time-step of $5e-4$ s and 6 maximum inner iterations. Thanks to this improvement, the simulation time was consistently decreased.

At this point it was possible to make some estimation of the time the simulation needed to be run. The initial aim of this thesis was to run the transient and Semi-Transient cases for at least 15 minutes of physical time. This is because test results show that in this time span most of the thermal phenomena have taken place and SS conditions are usually reached. Moreover, in this way it is possible to compare the simulations with the SS cases as well. However, time calculations showed that to simulate 15 minutes of the transient simulation, around two months and an half were necessary. After realizing this, it was decided to simulate less time due to the time-constraints imposed by the thesis. At the end, to be able to gather and analyze data, 4 minutes were simulated for all the cases. It was also decided to keep running the transient simulation after the thesis completion. It is recommended to proceed with the work according to the guideline and suggestions for future work presented in Chapter 5. Table 3.10 shows the solver's settings for the reference transient simulation.

Table 3.10: Transient Simulation Solver's Settings

Time	TS	MII	FF	BC
0-1.1 s	6e-5	4	no	Set1
1.1-60 s	5e-4	6	no	Set1
60-120 s	5e-4	6	no	Set2
120-180 s	5e-4	6	no	Set3
180-240 s	5e-4	6	no	Set4

3.7.3 Semi-Transient Simulations

Semi-Transient simulations are carried out with the aim to reproduce the same results of the transient one involving a lower computational time demand. This can be identified as the core of the project and as the main goal.

In Section 3.7.2, it was observed that the factors that affect the most the time efficiency of the transient simulation are Time-Step (TS) and Maximum inner Iterations (MII). Therefore, these are the parameters that need to be used to try to reduce the computational time demand of the simulations. The concept that was used for the definition of Semi-Transient simulations is that it can be observed that the flow field is stabilizing at a faster rate than the thermal one.

Using this observation, the idea is to first run the simulation with a smaller time-step and then increasing it once the flow stabilizes. The tracking and observation of different engineering quantities helped to understand when the flow was likely to be stable enough to increase TS. Since boundary conditions are changing each minute for the first three minutes, this procedure has to be implemented every time the boundary conditions where changed. The flow can be frozen using the solver's option *Segregated Flow: Freeze Flow* (FF) in STAR CCM+. By assuming different time-step sizes and settling times for the flow field, four different cases where identified for Semi-Transient simulations and they will be compared to the reference transient case. Tables 3.11a, 3.11b, 3.11c and 3.11d show the different solver conditions used for Semi-Transient simulations 1, 2, 3 and 4 respectively.

Table 3.11: Semi-Transient Simulations Solver's Settings**(a)** Semi-Transient 1

Time	TS	MII	FF	BC
0-0.4 s	6e-5	4	no	Set1
0.4-60 s	9e-3	6	yes	Set1
60-60.8 s	6e-5	4	no	Set2
60.8-120 s	9e-3	6	yes	Set2
120-120.8 s	6e-5	4	no	Set3
120.8-180 s	9e-3	6	yes	Set3
180-180.8 s	6e-5	4	no	Set4
180.8-240 s	9e-3	6	yes	Set4

(b) Semi-Transient 2

Time	TS	MII	FF	BC
0-0.4 s	5e-4	6	no	Set1
0.4-60 s	9e-3	6	yes	Set1
60-60.4 s	5e-4	6	no	Set2
60.4-120 s	9e-3	6	yes	Set2
120-120.4 s	5e-4	6	no	Set3
120.4-180 s	9e-3	6	yes	Set3
180-180.4 s	5e-4	6	no	Set4
180.4-240 s	9e-3	6	yes	Set4

(c) Semi-Transient 3

Time	TS	MII	FF	BC
0-0.8 s	5e-4	6	no	Set1
0.8-60 s	9e-3	6	yes	Set1
60-60.8 s	5e-4	6	no	Set2
60.8-120 s	9e-3	6	yes	Set2
120-120.8 s	5e-4	6	no	Set3
120.8-180 s	9e-3	6	yes	Set3
180-180.8 s	5e-4	6	no	Set4
180.8-240 s	9e-3	6	yes	Set4

(d) Semi-Transient 4

Time	TS	MII	FF	BC
0-0.8 s	6e-5	4	no	Set1
0.8-60 s	9e-3	6	yes	Set1
60-60.8 s	5e-4	6	no	Set2
60.8-120 s	9e-3	6	yes	Set2
120-120.8 s	5e-4	6	no	Set3
120.8-180 s	9e-3	6	yes	Set3
180-180.4 s	5e-4	6	no	Set4
180.4-240 s	9e-3	6	yes	Set4

3.8 Simulations Logic

The underlying theory for Steady State and Transient simulations have been explained in Section 2.9 and they are very well consolidated types of simulations that are used many times in engineering practice. In general, SS simulations are used to simulate and obtain the system behaviour at the equilibrium, while transient simulations are used to observe its behaviour during physical time. The concept of Semi-Transient simulations was developed during the thesis with the aim of achieving the same results of a transient simulation but in less computational time. The methodology used to achieve this last simulation type was described in Section 3.7.3 and it is the core of the project. Thus, it can be deduced that two very important perspectives to check are the actual time the simulations need to run and how the results will be compared to understand if Semi-Transient simulations are close in accuracy to the transient one and to which extent some of them can be used in real practice.

3.8.1 Time Estimations

Transient simulations are not used, when possible, in common practice due to their long computational time demand. In this project due to the large domain, complex model and very long solving time, transient simulations will take a very high amount of time to run and it may become unfeasible to use them in daily practice [6]. For this reasons, it has been attempted to find a solution by defining and experimenting a Semi-Transient method. If

successful, it will be possible to observe the system's behaviour over time with an acceptable degree of accuracy and involving a much lower time demand for computation. Table 3.12 shows the time required for the transient simulation to run to simulate 4 minutes, detailed for each minute, and an estimation of how long it would take to simulate 15.

Table 3.12: Transient Simulation Times

Physical time	Simulation time
0-1.1 s	25 h
1.1-60 s	118 h
60-120 s	120 h
120-180 s	120 h
180-240 s	120 h
Total 4 min	21 days
Total 15 min	76 days

For what concerns time demands for the four Semi-Transient cases, Tables 3.13a, 3.13b, 3.13c and 3.13d show them for Semi-Transient simulations 1, 2, 3 and 4 respectively for simulating 4 and 15 minutes. It is important to take carefully into consideration the estimation made for 15 minutes, as it has as assumption that the flow is kept frozen until the end. Further discussions about implications of this and different future approaches are presented in Chapter 5.

Table 3.13: Semi-Transient Simulations Time

(a) Semi-Transient 1

Physical time	Simulation time
Total 4 min	3.4 days
Total 15 min	5.4 days

(b) Semi-Transient 2

Physical time	Simulation time
Total 4 min	0.9 days
Total 15 min	2.9 days

(c) Semi-Transient 3

Physical time	Simulation time
Total 4 min	1 days
Total 15 min	3 days

(d) Semi-Transient 4

Physical time	Simulation time
Total 4 min	1.7 days
Total 15 min	3.7 days

It is important to note that the discussions following will regard only the first four minute span, which are the focus of the project. For considerations about the complete 15 minutes, please refer to Chapter 5. By observing the time estimations, time savings are from 84 to 96%. This could have a great positive impact on daily engineering projects. Thus, the next step is to compare the simulations to verify if the results are close to those of the reference transient case. The procedure implemented for the comparison is described below.

3.8.2 Comparison Method

Different post processing tools were used for the various simulations to help the analysis and comparison of results. Scenes were built with different focus, both for velocities and temperature

variables. For some of them, three different velocity and temperature intervals were chosen to analyze different parts. A list of the scenes together with their range is presented in Table 3.14.

Table 3.14: List of scenes printed

Scene Name	T [$^{\circ}\text{C}$]	v [m/s]	Scene Name	T [$^{\circ}\text{C}$]	v [m/s]
Absorbers surface	80-160	-	Overall car high	27-850	0-70
Engine bay high	27-850	0-20	Overall car mid	27-150	0-40
Engine bay mid	27-200	0-40	Overall car low	27-88	0-20
Engine bay low	27-160	0-70	RC1	85-150	-
Exhaust sections	27-850	0-200	RC2	84-180	-
Exhaust stones	80-850	0-70	Solids scene 1	50-777	-
Exhaust turbo	80-850	0-70	Solids scene 2	70-720	-
Fan inlet	72-83.5	-	Turbo-manifold	300-750	-
Fan outlet	76-86	-	Windtunnel high	27-200	0-50
HXCs and fan	27-90	0-25	Windtunnel mid	27-90	0-30
Lambda sensor	83-765	-	Windtunnel low	27-40	0-15

Where RC1 and RC2 are the rubber cylinders between the exhaust system and the adiabatic box and between the exhaust system and the turbo respectively. Each of the scenes were printed every one second of physical time simulated and stored in corresponding folders. These are used for comparison between cases and to create animations.

Many different plots were built as well in the model to keep track of various engineering quantities, such as temperatures, velocities, Courant number, residuals etc. Plots were particularly useful to check the convergence of SS simulations and to find the right combination of time-step and maximum inner iterations for the Transient and Semi-Transient cases. Plots are a very powerful tool to use during the simulations' run to keep track on the progress of the simulations and to spot unrealistic physics behaviour, when occurring. Temperatures of different components were gathered together in a single plot to facilitate visualization, for example for solids. Moreover, it is possible to obtain different types of plots by imposing different types of monitors, such as maximum temperature, average temperature and many others.

However, plots themselves are not practical for comparison between simulations since it is not possible to put the same plots for each simulation in the same graph. Thus, a different method has to be used to compare engineering quantities' behaviour in the different simulations. Moreover, it is also important to define which quantities and components are necessary to keep track of, and to reduce their number at the minimum possible not to overfill the simulation files with unnecessary post-processing features. After a careful analysis, eleven different components were selected for further comparison between the simulations. For each of these components, spheres were created in the *Derived Parts* section in STAR CCM+ server. Temperatures for these spheres were decided to be the tracked engineering quantities to observe and compare since the focus of this project is on the thermal profiles of the underhood compartment. Table 3.15 shows the different components selected and the number of spheres on each of them selected as evaluation points.

Table 3.15: List of spheres for further comparison

Component	Number of Spheres
Air after fan	9
Exhaust gas	10
First catalyst's insulated areas	18
First catalyst's non-insulated areas	9
Turbo and manifold	11
Rubber cylinder between exhaust system and adiabatic box	6
Rubber cylinder above the gear box	6
Rubber cylinder between exhaust system and turbo	6
Heat shield	10
Upper absorber	5
Lower absorber	5

To see the position of the spheres in each component, please refer to Appendix A.3. The choice of the position of the spheres was decided by looking at SS scenes to identify the hotspots. For each sphere, reports, monitors and plots were created. For the analysis and comparison of the different simulations, monitors are very important. In particular, by extracting the monitors for all the spheres, it is possible to gather the same spheres monitors for the different simulations in a common plot by the use of Excel. Three different Excel sheets have been created due to the huge amount of data processed. The sheets were created before the end of the simulations. This was possible by creating different Java Macros for the extraction of the monitors for each of the eleven components and creating the links in Excel with the exported files. In this way, once all the simulations were completed, it was necessary only to run the eleven macros in each simulation file and refresh the connections in Excel. Then for each sphere's monitor a graph of its temperature behaviour in the simulations was created. In total, considering each sphere of each components, 95 graphs were obtain to compare. In each graph, monitors for the SS, Transient and 4 Semi-Transient Simulations have been gathered. It is important to note that the comparison with the SS simulation cannot be made due to the time constraint for the project. Therefore, its representation in the plot's will be omitted for the scope of this project.

4

Results

As already highlighted in Section 3.8.2, different post-processing tools have been used in the project such as scenes, plots and monitors. As a result, it was possible to collect a very wide variety of results and information about the transient simulation and the four semi-transient ones. Using monitors with the methodology explained in Section 3.8.2, plots for all the simulations considered could be made for each sphere. An example of the type of plots obtained is shown in Figure 4.1.

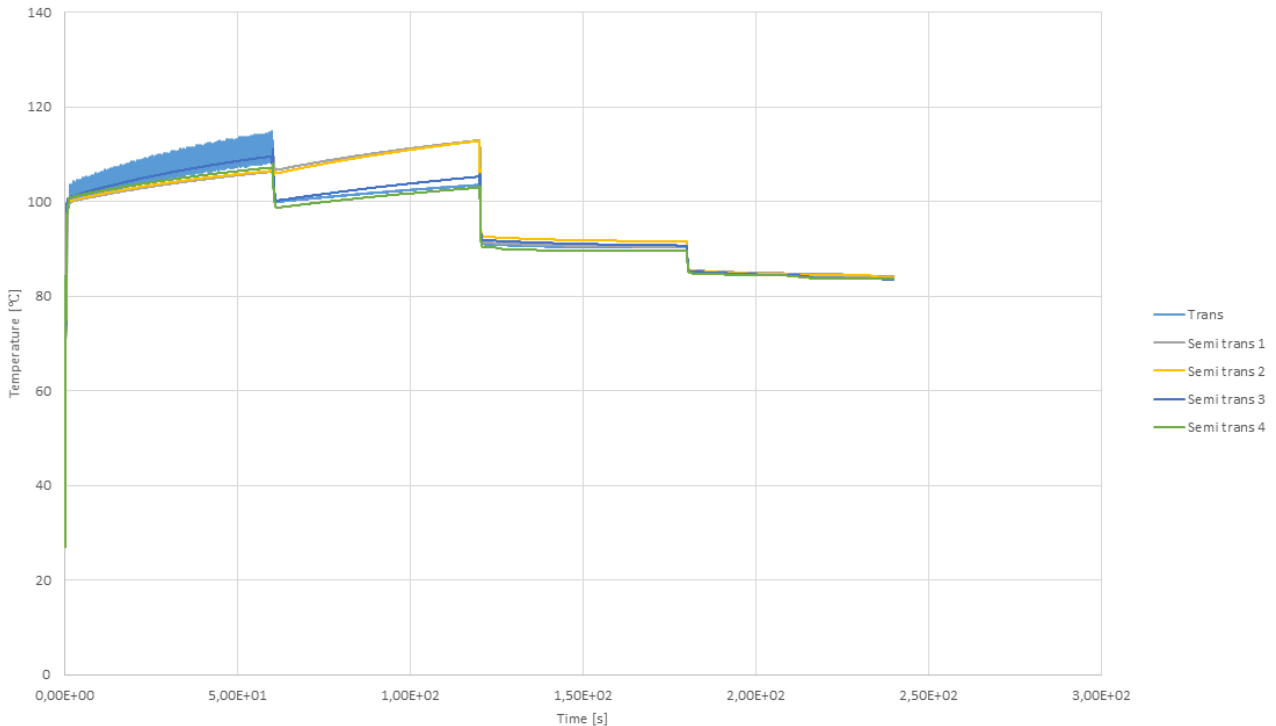


Figure 4.1: Plot example, sphere 27 01 in heat shield component

As it can be seen, two different aspects can be considered. One is the final value reached by each semi-transient simulation at the end of the fourth minute and the difference for each of them with respect to the final value reached in the transient simulation. The other aspect that can be observed is whether each semi-transient simulation has a similar path during the four minutes as the one of the transient simulation.

For now, the first aspect will be the one analyzed and considered as most important. For each sphere, the differences between each of the final semi-transient values and the transient final

values are calculated. These will be referred to from now on as errors. With this data, it was possible each of the 11 component was analyzed in the same way. Based on the errors calculated, the relative and absolute errors for each semi-transient simulation, together with the maximum error for each of them, could be calculated. The formula used to make these calculations are shown in Equations 4.1 and 4.2. Please note that RE, AE and ME stand for relative error, absolute error and maximum error respectively. For each component:

$$RE_i = \frac{\sum_{j=1}^{n_{spheres}} error_{ij}}{n_{spheres}} \quad (4.1)$$

$$AE_i = \frac{\sum_{j=1}^{n_{spheres}} |error_{ij}|}{n_{spheres}} \quad (4.2)$$

Where i is the index defining the semi-transient simulations and it goes from 1 to 4. For what concerns the ME, if-loops were used in Excel to identify between each sphere of the component analyzed which was the biggest error. The if-loops were used to be able to consider also negative values. Considering the semi-transient simulations together, average deviation was calculated in each component for each type of error. Average deviation, AD, was calculated for each error type k according to equation 4.3.

$$AD_k = \frac{\sum_{i=1}^4 |error_{ik}|}{\sum_{i=1}^4 \left(\frac{error_{ik}}{error_{ik}+0.000000001} \right)} \quad (4.3)$$

The resulting errors and average deviations for each semi-transient simulation for each component are shown below.

Table 4.1: Air after fan component

Simulation	RE	AE	ME
Semi-Transient 1	-0.01	0.09	0.18
Semi-Transient 2	-0.53	0.53	-0.68
Semi-Transient 3	-0.58	0.58	-0.72
Semi-Transient 4	-0.61	0.61	-0.73
Average Deviation	0.43	0.45	0.58

Table 4.2: Exhaust gas component

Simulation	RE	AE	ME
Semi-Transient 1	0.76	0.85	2.76
Semi-Transient 2	-2.84	3.41	-13.93
Semi-Transient 3	-4.29	4.84	-10.21
Semi-Transient 4	2.25	2.26	11.77
Average Deviation	2.54	2.84	9.67

Table 4.3: CAT insulated area

Simulation	RE	AE	ME
Semi-Transient 1	-1.90	3.06	-17.62
Semi-Transient 2	-6.32	10.01	-27.86
Semi-Transient 3	-0.14	1.85	11.17
Semi-Transient 4	1.22	4.29	14.49
Average Deviation	2.40	4.80	17.78

Table 4.4: CAT non insulated area

Simulation	RE	AE	ME
Semi-Transient 1	-0.77	4.97	-21.28
Semi-Transient 2	-2.19	4.78	-15.87
Semi-Transient 3	-6.03	6.58	-8.88
Semi-Transient 4	2.32	3.44	7.22
Average Deviation	2.83	4.94	13.31

Table 4.5: Turbo and manifold

Simulation	RE	AE	ME
Semi-Transient 1	0.34	4.09	-12.31
Semi-Transient 2	-0.25	1.51	-3.30
Semi-Transient 3	-5.47	7.59	-12.07
Semi-Transient 4	1.39	2.77	9.89
Average Deviation	1.86	3.99	9.39

Table 4.6: RC above gear box

Simulation	RE	AE	ME
Semi-Transient 1	-0.59	0.59	-0.71
Semi-Transient 2	-1.11	1.11	-1.22
Semi-Transient 3	-1.27	1.27	-1.41
Semi-Transient 4	-1.33	1.33	-1.46
Average Deviation	1.07	1.07	1.20

Table 4.7: RC exhaust-adiabatic box

Simulation	RE	AE	ME
Semi-Transient 1	0.80	1.40	2.70
Semi-Transient 2	2.42	2.42	3.54
Semi-Transient 3	2.09	2.09	3.03
Semi-Transient 4	0.51	1.02	2.49
Average Deviation	1.45	1.73	2.94

Table 4.8: RC exhaust-turbo

Simulation	RE	AE	ME
Semi-Transient 1	-1.48	1.57	-4.32
Semi-Transient 2	0.48	2.01	3.98
Semi-Transient 3	-0.68	0.74	-1.41
Semi-Transient 4	-1.09	1.47	-2.15
Average Deviation	-0.69	1.45	-0.97

Table 4.9: Upper absorbent

Simulation	RE	AE	ME
Semi-Transient 1	0.08	0.18	0.39
Semi-Transient 2	-0.81	0.81	-2.16
Semi-Transient 3	-0.69	0.69	-1.59
Semi-Transient 4	-0.62	0.63	-1.59
Average Deviation	-0.51	0.58	-1.24

Table 4.10: Lower absorbent

Simulation	RE	AE	ME
Semi-Transient 1	0.33	0.52	2.00
Semi-Transient 2	-2.83	2.83	-8.00
Semi-Transient 3	-0.42	0.42	-0.78
Semi-Transient 4	0.68	0.95	2.56
Average Deviation	-0.56	1.18	-1.05

Table 4.11: Heat shield component

Simulation	RE	AE	ME
Semi-Transient 1	-1.53	1.53	-3.37
Semi-Transient 2	-0.51	1.96	-6.51
Semi-Transient 3	-0.92	0.92	-1.70
Semi-Transient 4	-1.08	1.97	-6.28
Average Deviation	-1.01	1.59	-4.47

In the tables from 4.1 to 4.11, color coding was used to highlight the most critical errors. According to the components analyzed, different values should be used to define the acceptable and critical areas. Overall, two different scales were used, from now on referred to as Scale 1 and Scale 2. For each scale, three intervals were defined, highlighted in green, yellow and red. Green cells therefore identify error values that are acceptable, yellow are errors that are almost acceptable, and red error values are more critical and should be investigated to understand if the semi-transient simulation associated to them is accurate enough. The two scales used

together with the components that use them are shown in Table 4.12. This colour coding was implemented for all the types of error (RE, AE and ME).

Table 4.12: Scales used for error classification

Scale	Green	Yellow	Red	Components
Scale 1	$-5 < x < 5$	$5 < x < 10$ $-10 < x < -5$	$x > 10$ $x < -10$	Fan, RC1, RC2, RC3, upper, lower absorber
Scale 2	$-15 < x < 15$	$15 < x < 30$ $-30 < x < -15$	$x > 30$ $x < -30$	Exhaust gas, CAT insulated, non insulated, turbo and manifold

The reason why two scales have been used is that the 11 components chosen are not all at the same temperature range. Components such as the catalysts insulated and non insulated areas, exhaust gas flow, turbo and manifold are reaching very high temperatures. For this reason, a higher error can be allowed for them as it will be compared to the already high temperatures they reach. Now that the most critical values can be analyzed to understand if the semi-transient method developed is a good option to replace the transient one in daily practice and if so, it can be considered which semi-transient simulation showed the best overall results over physical time.

First, no red cells are present, highlighting an overall good quality of results for all the semi-transient cases. Observing the yellow cells, that represent errors that are still acceptable but not optimal, the biggest and most concerning variation from transient results are in the CAT insulated and non insulated areas, especially concerning the ME for semi-transient simulations 1 and 2. The average deviations for the CAT insulated and non insulated areas are 17.78 and 13.31, and it is possible to notice that they are mainly caused by the high ME for semi-transient simulations 1 and 2 respectively. Under this perspective, it seems that semi-transient simulations 1 and 2 fail to describe some flow features and engineering quantities in a precise way in particularly sensitive areas among the ones considered now. For this reason, they are likely not be the best of the four semi-transient simulations, even though their efficiency in predicting resulting is still high. Thus the choice of the best semi-transient simulation should relate either semi-transient simulation 3 or 4.

The average deviations shown for semi-transient simulations 3 and 4 highlight that both these simulations involve small errors compared to results from the transient simulation. Thus, other aspects have to be considered to make a decision of which is the best semi-transient simulation. At the beginning of this Chapter, two aspects have been mentioned as important for the analysis. The first one, regarding the errors calculated at the end of the 4 minutes, has been considered, leaving semi-transient simulation 3 and 4 to be selected. Now, the second aspect that was described will be used, which consisted of observing how the simulations behave during the simulation time with respect to how the transient case behaves. The plots developed in Excel, as the one shown in Figure 4.1 previously, are very useful for this purpose. All the post-processing plots created in Excel have been revised to check the behaviours and trend of simulations during physical time. Overall, a specific trend could be seen: semi-transient simulation 4 seems to follow a more different path than semi-transient 3 with respect to the transient simulation. This can be seen in many plots of different components. As examples,

four different plots are shown for spheres in four different components to substantiate the observations made. They are shown in Figures from 4.2 to 4.5.

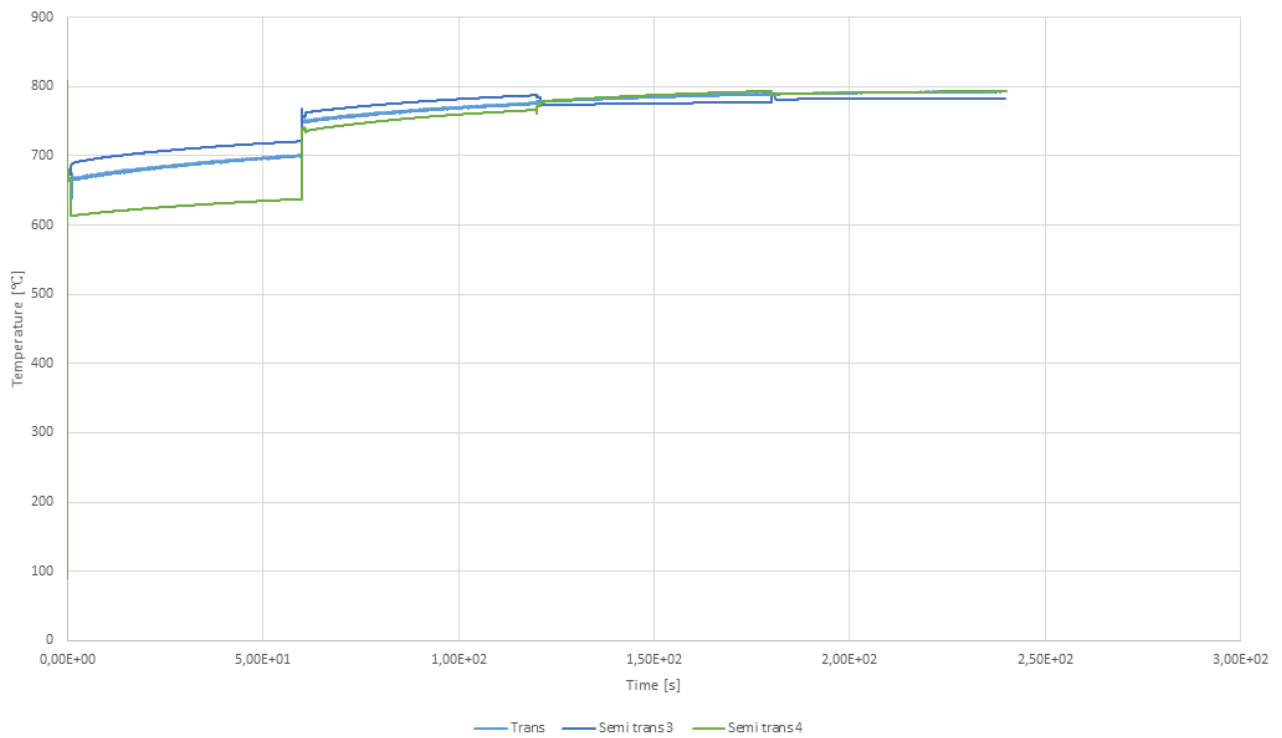


Figure 4.2: Sphere 24 05, exhaust gas component

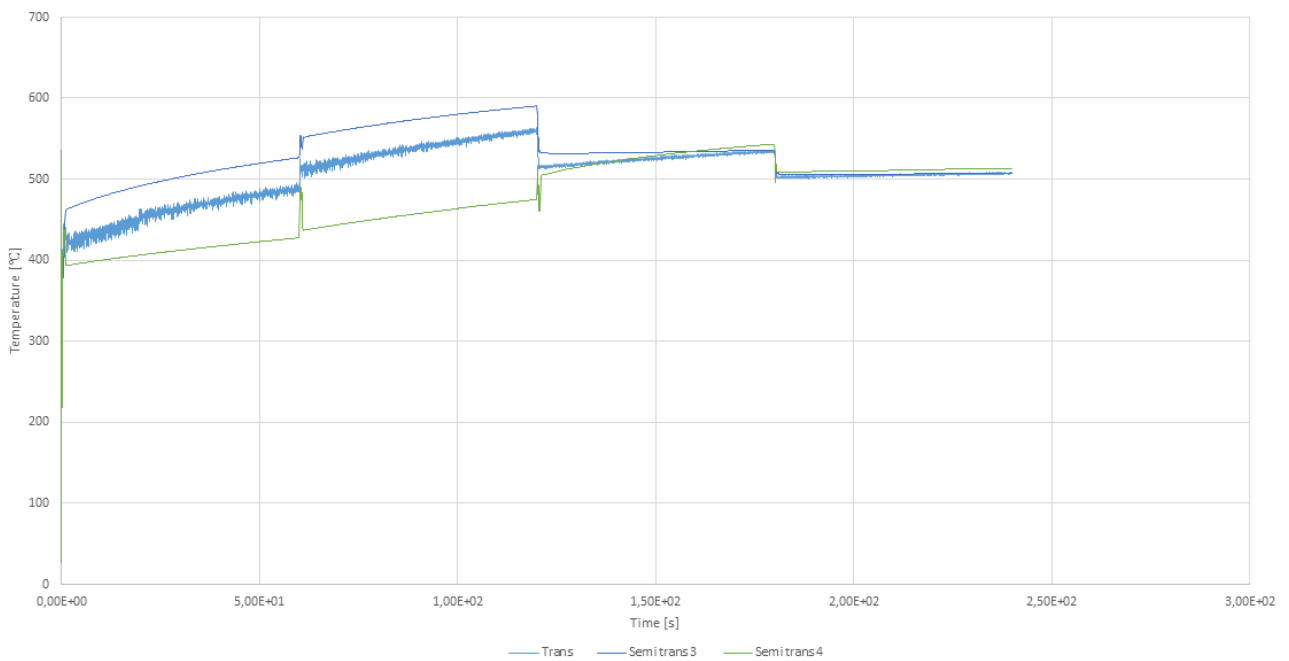


Figure 4.3: Sphere 25 02, CAT insulated

4. Results

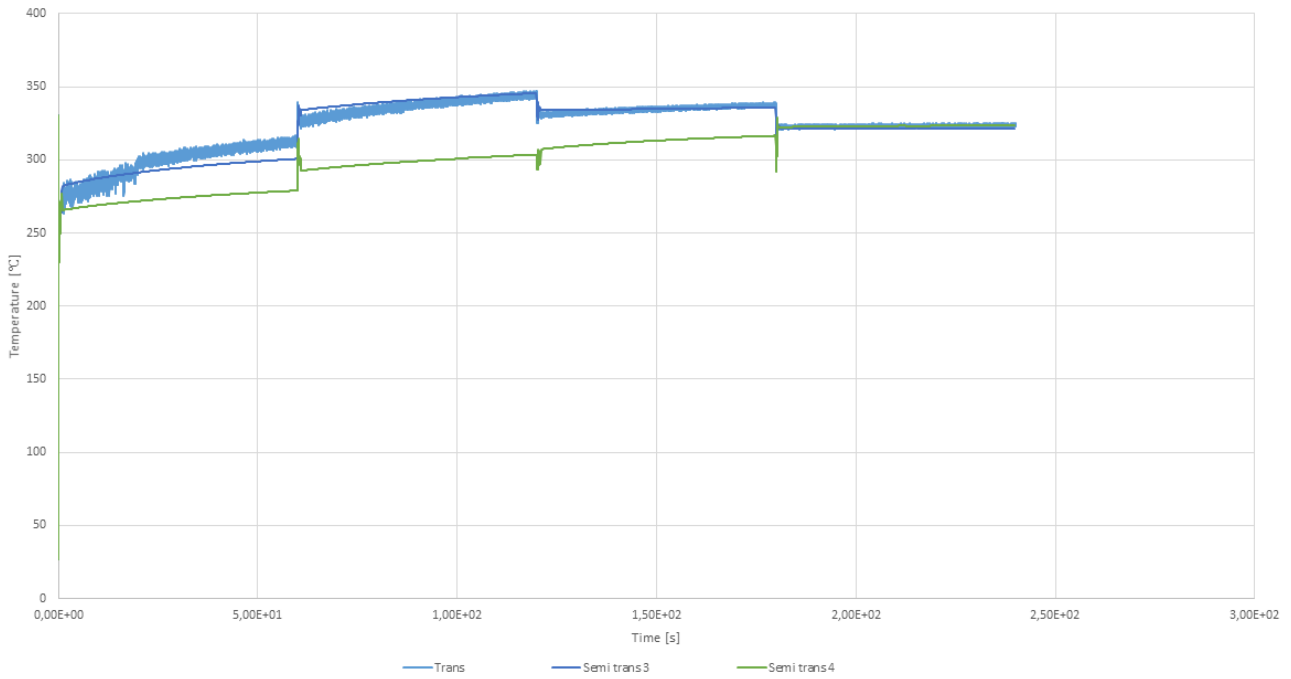


Figure 4.4: Sphere 26 01, CAT non insulated

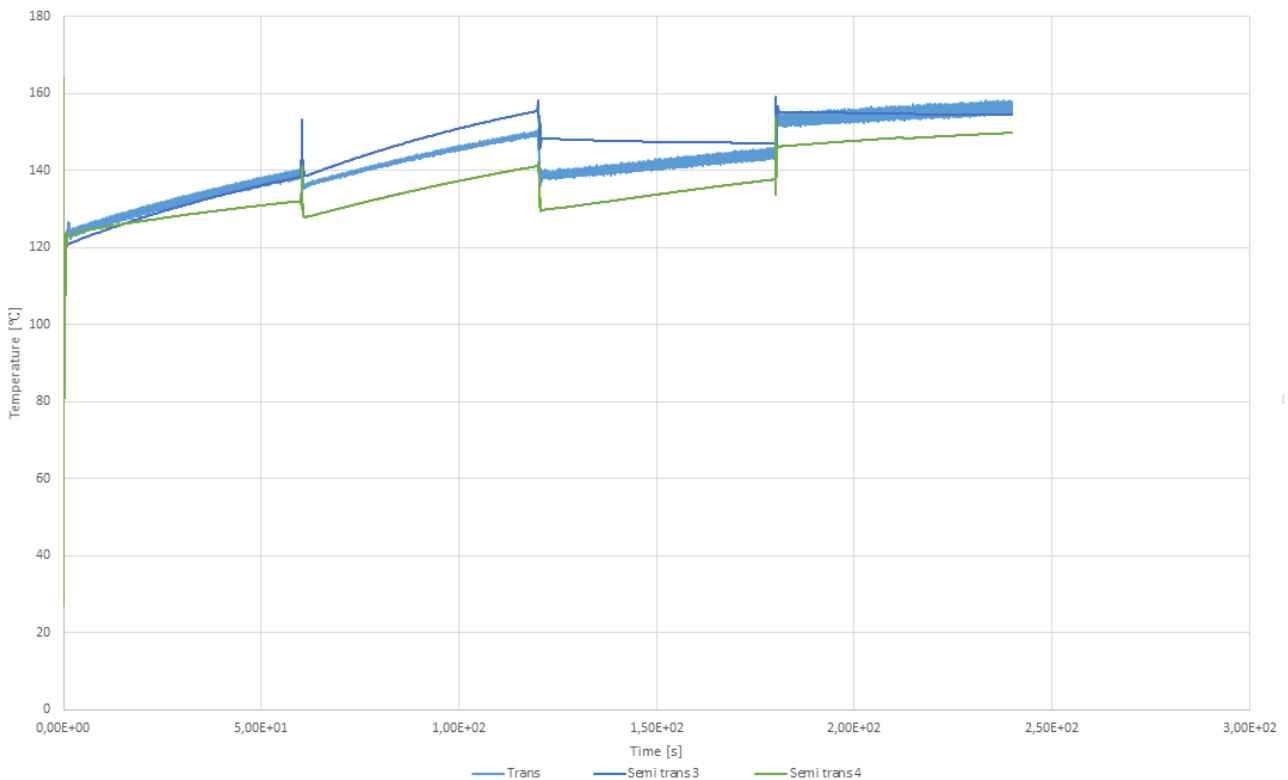


Figure 4.5: Sphere 27 08, heat shield component

As it is possible to observe, semi-transient simulation 4, in green, follows the reference transient simulation less accurately during physical time compared to semi-transient 3, in

dark blue. For all the reasons explained in this Chapter, semi-transient simulation 3 seems to be the best simulation to reproduce the reference transient simulation with less computational time. Regarding the computational time involved, the choice of semi-transient simulation 3 is very beneficial as its simulation time is one of the smallest one, as shown in Table 3.13c.

There are however some questions that need to be considered, especially regarding semi-transient simulation 4. As it can be seen in Tables 3.11, observing the delta time, time-steps and maximum inner iterations, it seemed likely that semi-transient simulation 4 was expected to give better results and smaller errors. This is due to the fact that in the first minute, the first 0.8 seconds were run using a smaller time-step equal to the one of the transient simulation, while semi-transient 3 used a larger one. It is thus important to investigate the causes for which semi-transient 4 results do not better reproduce transient simulation results. For this purpose, the plot for sphere 26 01 in the CAT non insulated area is used. First a zoom into the first 10 seconds of physical time has been made and it can be observed in 4.6.

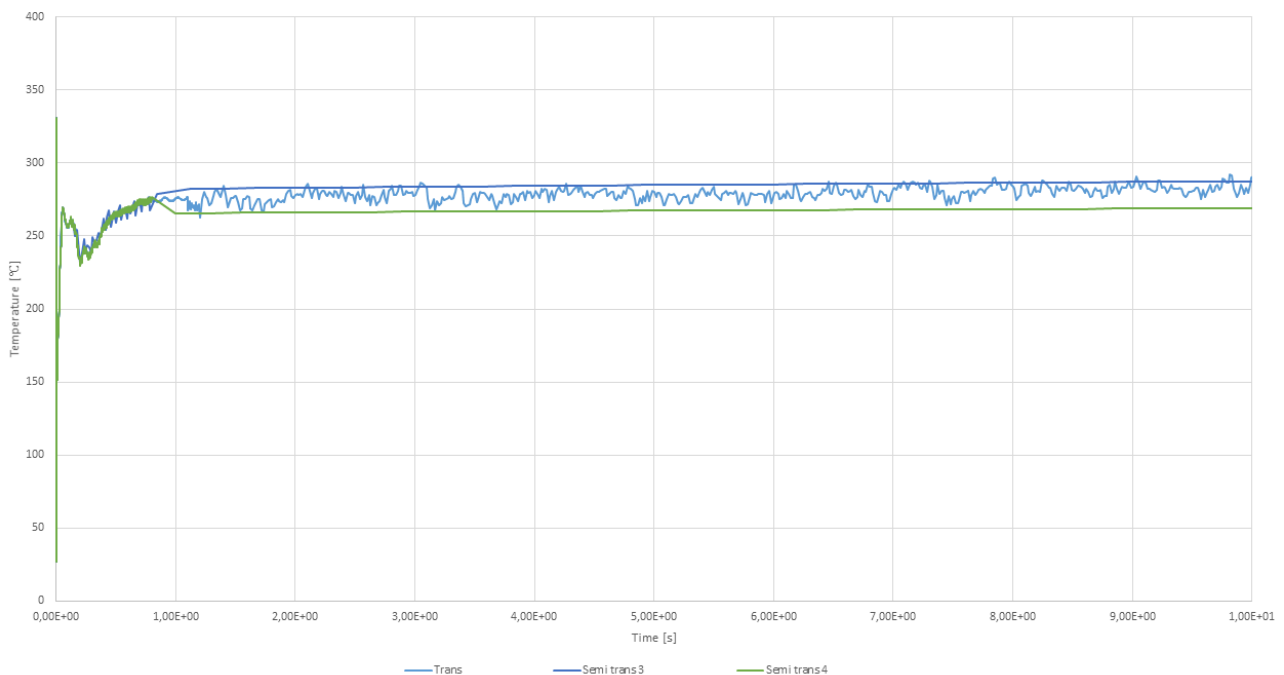


Figure 4.6: Zoom of the first 10 seconds, sphere 26 01

As it is possible to see, in the first seconds it seems that both semi-transient 3 and 4 followed the reference transient simulation path, but then semi-transient simulation 3 seems to start taking another direction, arriving at the final result shown in Figure 4.4. Thus, something must have happened in that first short time span. For this reason, a further zoom on the first 1.5 seconds of the physical time has been made and it is shown in Figure 4.7.

4. Results

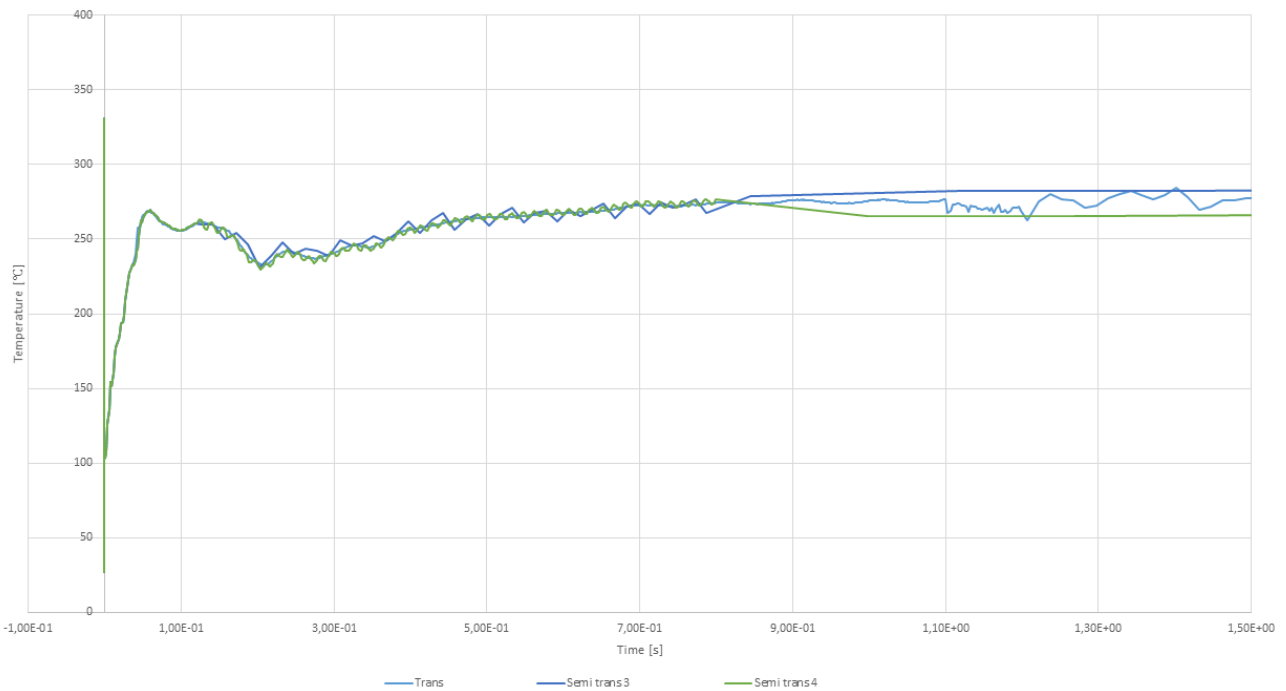


Figure 4.7: Zoom of the first 1.5 seconds, sphere 26 01

From Figure 4.7, it is possible to notice interesting patterns. In particular, in the first 0.8 seconds semi-transient simulation 4 follows much more the transient path, by oscillating around it at a higher frequency than semi-transient 3. However, after the first 0.8 seconds, when the flow field is frozen, semi-transient 4 seems to start diverging from the transient path, leaving semi-transient 3. Two possible reasons have been formulated as possible explanations for this behaviour. One can be that freezing the flow at 0.8 might have been a too early choice, and the intrinsic lower stability of semi-transient 4 due to the smaller TS compared to semi-transient 3 might have had a negative effect on the following minutes of simulation. Another reason can be instead that a lower time-step is actually not beneficial for this case. This is due to the fact that the higher oscillations rate of semi-transient 4 could increase the risk of being at the top or at the bottom of the wave when freezing the flow, changing the simulation results to a greater extent. It is recommended to further investigate these reasons, by for example observing how semi-transient 4 would behave if more time was allowed for the flow field to stabilize. This will be discussed in greater detail in Chapter 5.

5

Future Work Suggestions

In Chapter 4, the analysis of the data obtained from the different simulations was performed, and semi-transient simulation 3 was chosen to be the best to reproduce transient results. However, it was also highlighted that some improvements could be made for semi-transient simulation 4, which was expected to show closer results to the reference transient simulation. The reader can also recall that one of the limitations of this project was the inability to run the simulations for the desirable amount of physical time, which was 15 minutes. This was caused by the time constraints imposed by the project. Thus, all the analysis made refers to the first 4 minutes of physical time. It is also important to remember that Boundary Conditions have been changed in the first four minutes of the simulation, as explained in Section 3.6.2 and shown in Figure 3.15 and Table 3.7. These minutes can be seen as the time frame in which all of the changes in BC occur. After that, no further changes are present and the simulation will be to a certain extent more stable and involving less sharp changes in the flow and thermal fields. For all these reasons, the next question would be how to proceed from now on with the simulations. This section is thus written with the aim of giving suggestions of how the future work of the thesis can be structured and which aspects need to be studied next.

The suggestions for future work can be divided into two main phases, one concerning improvements in the first minute of simulation of the physical time and the second concerning how to proceed after the completion of the first four minutes simulation. The semi-transient methodology, explained in Section 3.7.3, was based on the observation that it was possible to freeze the flow after some time due to the fact that it was stabilizing at a faster rate than the thermal field. This method seems to have worked very well for all the semi-transient simulations, especially number 3. The first suggestion that can be made concerns which simulations should be run in the future. A suggestion is to rerun semi-transient 4 in the first minutes by allowing more time before freezing the flow field, for example 4 seconds. In this way it is possible to see how results are changed and if it could be the best simulation to represent the transient results or if 3 is still better. Another aspect that can be investigated regarding the first four minutes of physical time is whether flow field needs in general to be updated two times every minute, one at the beginning and another time, maybe in the middle of the minute simulated. It is beneficial to analyze the effect that this has on the final error computation. For each case, it is important to update the calculation of the computational time needed.

After the first four minutes have been analyzed in this project, it is important to ask how to proceed with semi-transient methodology since no BC changes are occurring again. Should the flow be frozen from all the remaining minutes of physical time to simulate? Or should it

be updated by unfreezing it and freezing it again? If so, when and how often should the flow field be updated? And for how long? As it is possible to understand, there is still a very wide range of questions to investigate, and it is recommended to do so in a new project.

As the set of questions to answer is very wide, it is suggested to proceed with the comparison of only semi-transient simulation 3 and 4 with respect to the reference transient simulation. The transient simulation will continue to run after the end of the project as it represented the time-limiting aspect of this project and it will be the same for a future one. For this simulation, nothing has to be changed, it needs only to run until the physical time desired. Post-processing tools will still be available and monitor will only need to be exported again at the end using Java Macros and results could be seen and analyzed in the already compiled and used Excel document. For what concerns the monitors, it is also suggested to increase the number of time-steps before they are printed, to reduce the size of the Excel file to compare results. As an alternative a Java script was kindly written by Jacob Vikström, in which monitors files exported were reduced by only keeping every tenth value of the series.

Concerning the second phase, with which Semi-Transient simulation to proceed with will be better clear once the first phase of the future work has been completed. Thanks to Semi-Transient simulations' relatively low computational time demand, compared to the transient one, it is possible to investigate many different cases for the simulations, varying the frequency to update the flow field and the time allowed for the flow to be unfrozen. For example, one configuration should be the extreme case in which the flow field is not updated at all until the end of the 15 minutes. Another could be that it is only updated once for a period of 0.8s and so on. Thus, a design of experiments is needed to select which cases to run. Then all of them should be compared to transient results to understand which configuration is the best one that can be used in other cases of daily engineering practice as well.

The future work should be done by keeping in mind the aim of the project is to find a time-efficient option to get the same transient results of the case considered. In the analysis of the future work also the SS case could be included, since after 15 minutes SS conditions are assumed to be reached looking at wind tunnel test results.

6

Conclusion

After the results have been analyzed and discussed, it is possible to draw some major conclusions on the overall outcome of the project. In particular, these will answer to the research questions formulated in Section 1.5.

By observing the resulting post-processing data and computing the errors between the different semi-transient simulations and the transient reference one, it is possible to conclude that the semi-transient methodology developed throughout the project has revealed to be effective and able to reproduce transient results with a very good degree of accuracy. This methodology is based on the use of the *Freeze Flow* option in STAR CCM+. The four semi-transient cases presented are different from each other by using different values of time-steps, Maximum inner iterations number and time spans before freezing the flow. To recall the values, please refer to Table 3.11. Among the simulations made, the one that seems to be more similar to the reference transient case is number 3, even though some other investigations are recommended for semi-transient simulation 4.

Therefore, a future layout of the work to be done can be divided into two phases. The first one concerning a further analysis of the first four minutes of simulation for semi-transient 3 and 4, with a particular focus on the frequency and duration for which the flow field is updated. The second phase concerns the definition of a new design of experiments for the remaining minutes of the simulation, from minute 5 and onward. In this phase the focus should be on understanding when and for how long the flow field needs to be updated even if BC are not changing anymore. An optimal case should be found in this phase.

Bibliography

- [1] Zhang, C., Uddin, M., and Foster, L., *Investigation of the Under-Hood Aero-Thermal Flow Features Using 3D CFD Simulation*, SAE Technical Paper 2017-01-0142, 2017, doi:10.4271/2017-01-0142.
- [2] Khaled, M., Alshaer, A., Hachem, F., Harambat, F., and Peerhossaini, H., *Effects of Ground Vehicle Inclination on Underhood Compartment Cooling*, International Journal of Automotive Technology 13.6, pp.895–904, 2012, doi:10.1007/s12239-012-0090-8.
- [3] Seider, G., and Bet, F., Heid, T., Hess, U., Klein, T., and Sauer, J., *A Numerical Simulation Strategy for Complex Automotive Cooling Systems*, SAE Technical Paper, copyright:Society of Automotive Engineers, in: *The Proceedings of the 2001 Vehicle Thermal Management Systems Conference*, 2001, ISSN:0148-7191.
- [4] Xiao, G., Yang, Z., Wang, D., and Zhang, W., *Investigation of Radiation and Conjugate Heat Transfers for Vehicle Underbody*, SAE Technical Paper 0148-7191, 2008, ISSN:0148-7191.
- [5] Reister, H., and Bauer, W., *Simulation Process of the Heat Protection of a Full Vehicle*, SAE Technical Paper 2012-01-0635, 2012, doi:10.4271/2012-01-0635.
- [6] Shim, H.R., and Park, J.M., *A Study of the Transient Analysis Technique on the Under Hood Thermal Damage*, SAE Technical Paper, 2011, ISSN:0148-7191.
- [7] Binner, T., Reister, H., Weidmann, E.P., and Wiedemann, J., *10 Aspects of Underhood Thermal Analyses*, 2006.
- [8] Nimitan, R., Doost, A.K., and Maani, D., *Simulation of Air Flow under the Hood of a Passenger Car Using Computational Fluid Dynamics*, Research Journal of Applied Sciences, Engineering and Technology 6(24), pp.4583–4594, 2013, ISSN:2040-7459.
- [9] Hasegawa, T., *Simulation of the thermal underhood environment with CFD*, ATZ Worldwide 110.4, pp.24–28, 2008, <https://doi.org/10.1007/BF03224999>.
- [10] Zhang, C., Uddin, M., Song, X., Fu, C. et al., *Simultaneous Improvement of Vehicle Under-Hood Airflow and Cooling Drag Using 3D CFD Simulation*, SAE Technical Paper 2016-01-0200, 2016, doi:10.4271/2016-01-0200.
- [11] Andersson, B., Andersson, R., Håkansson, L., Mortensen, M., Sudiyo, R., and van Wachem, B., *Computational Fluid Dynamics for Engineers*, 13th edition, 2017, Internal Chalmers version.
- [12] Wilcox, D.C., *Turbulence Modelig for CFD*, 3rd edition, 2006, DCW Industries Inc., ISBN: 978-1-928729-08-2.
- [13] Versteeg, H.K., and Malalasekera, W., *A Introduction to COMPUTATIONAL FLUID DYNAMICS. The Finite Volume Method*, 2nd edition, 2007, Pearson Education Limited, ISBN: 978-0-13-127498-3.
- [14] Regin A.F., Agarwal, A., and Mishra, N., *Passenger Car Front End Optimization Using CFD Simulation*, SAE Technical Paper 2014-01-0627, 2014, doi:10.4271/2014-01-0627.

- [15] Hinze, J.O., *Turbulence*, 2nd edition, 1975, McGraw-Hill, ISBN:0-07-029037-7.
- [16] Çengel, Y.A., *Heat and Mass Transfer. A Practical Approach*, 3rd edition, 2007, McGraw-Hill, ISBN:978-0-07-312930-3.
- [17] Koizumi et al., *MRF Modeling of Axial Fan for Thermal Simulation of Electronic Equipment*, 2014, in: *Transactions of The Japan Institute of Electronics Packaging*, Vol. 7, No. 1, DOI: 10.5104/jiepeng.7.58.
- [18] Smith, R., *Moving Reference Frame for Computational Fluid Dynamics* [Blog post], 2013, June 24. Retrieved from <https://symscape.com/blog/moving-reference-frame-for-cfd>.
- [19] CD-adapco, *User guide STAR CCM+. Version 12.06.010*, Section: Simulating Physics, Modeling Porous Media.
- [20] Siemens Product Lifecycle Management Software Inc., CT09101_CM12_1, *STAR CCM+ Basic Training*, 2017, Section: Discussion, Effective simulations.
- [21] SAS IP, Inc., *1.2.1 Steady State and Transient Flows*. Retrieved from https://www.sharcnet.ca/Software/Ansys/16.2.3/en-us/help/cfx_mod/i1298451.html

A

Appendix

A.1 Computational Domain

In this section the overall computational domain for the project is presented, looking at it from different angles.

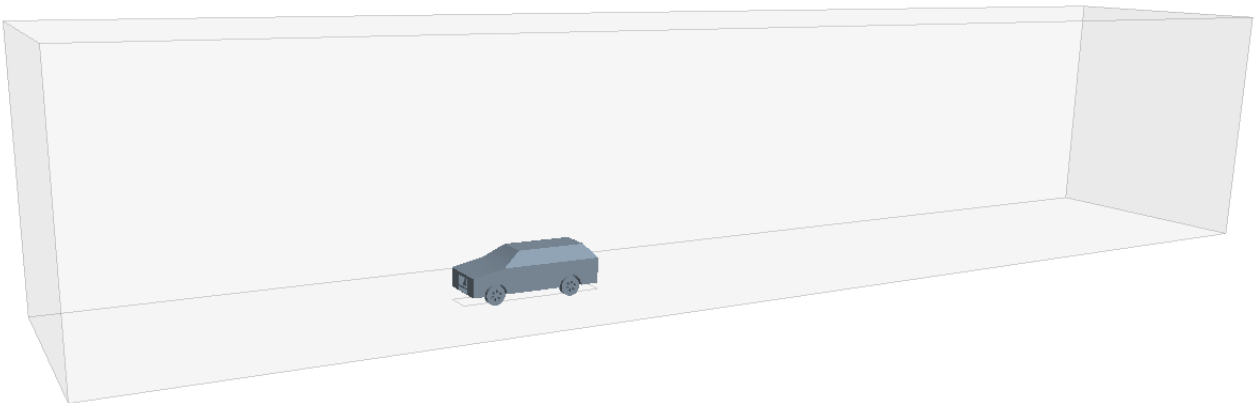


Figure A.1: Computational Domain, view 1

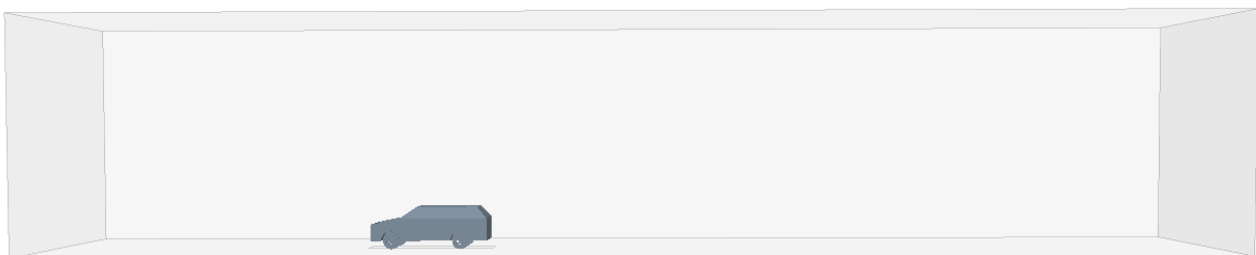


Figure A.2: Computational Domain, view 2



Figure A.3: Computational Domain, view 3

A.2 Refinement Blocks

In this section the refinement blocks used for the Fluid flow AM are presented in different colours in Figure A.4, A.5 and A.6

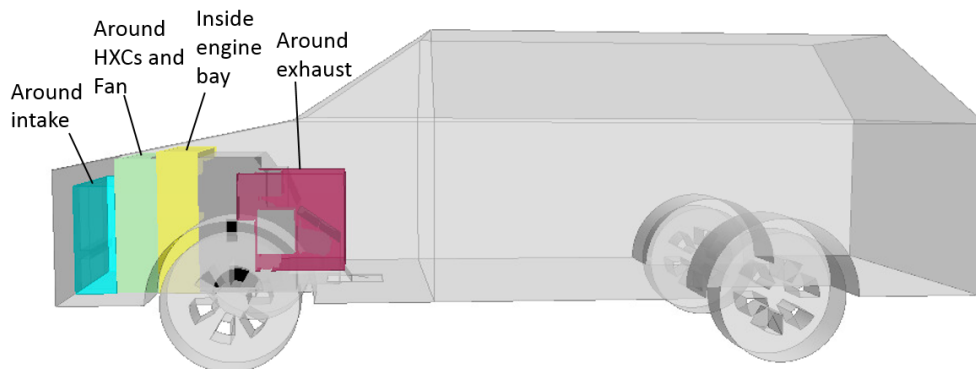


Figure A.4: Four refinement blocks

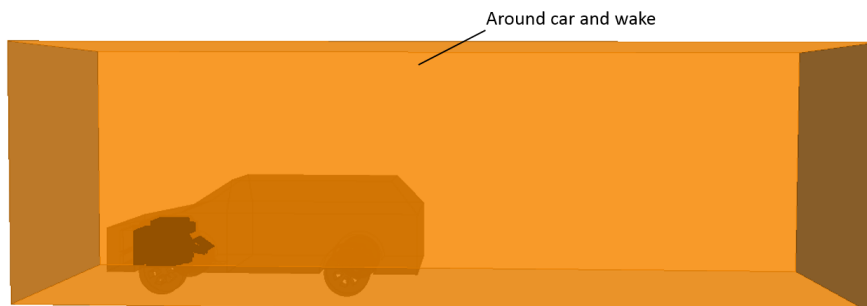


Figure A.5: Refinement block around the car and its wake

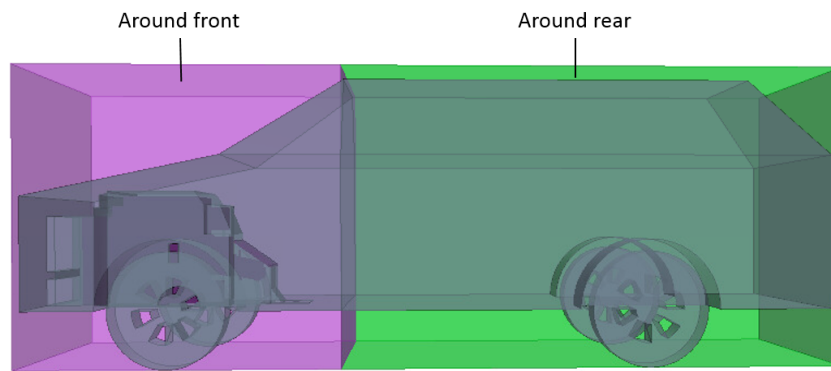


Figure A.6: Refinement block around the car's rear and front parts

A.3 Spheres Position

In this section is possible to observe the position of the spheres selected as evaluation points for each component.

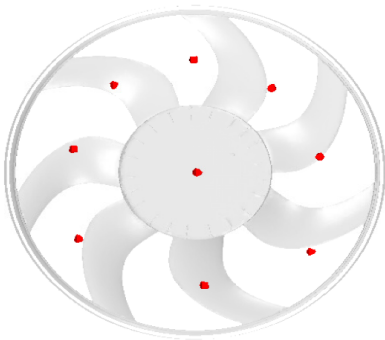


Figure A.7: Air after fan spheres

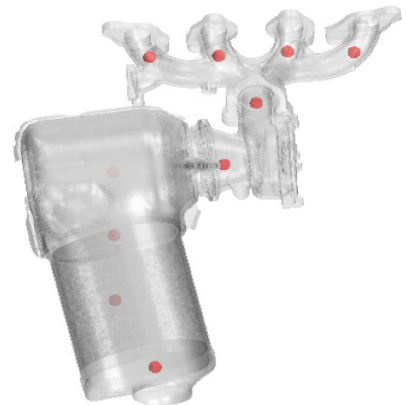


Figure A.8: Exhaust gas spheres

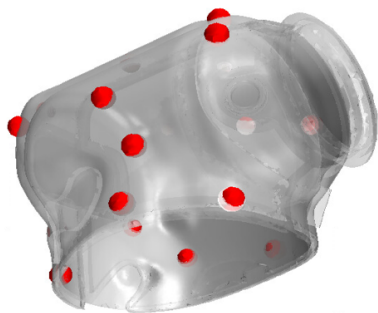


Figure A.9: CAT1 insulated spheres



Figure A.10: CAT1 non insulated spheres



Figure A.11: Spheres for the three RC

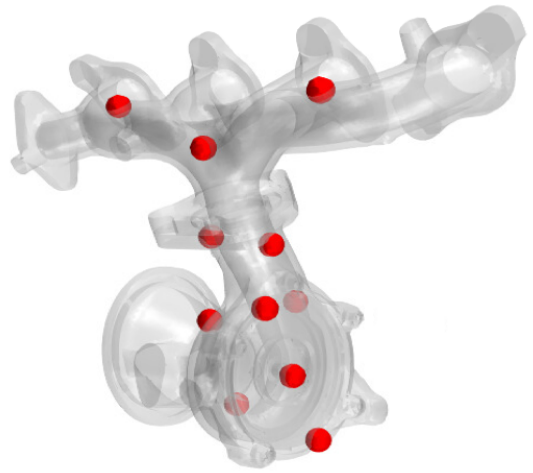


Figure A.12: Turbo and manifold spheres



Figure A.13: Heat shield spheres

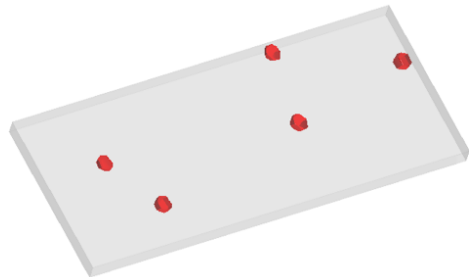


Figure A.14: Upper absorber spheres

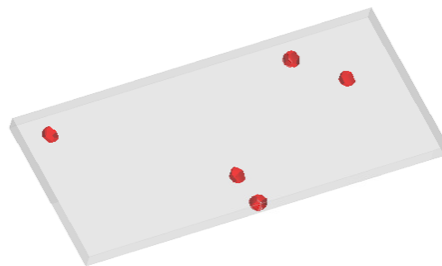


Figure A.15: Lower absorber spheres